Arch Comput Methods Eng (2008) 15: 277–309
DOI 10.1007/s11831-008-9021-2

ORIGINAL PAPER

A Survey on the Numerics and Computations for the Landau-Lifshitz Equation of Micromagnetism

Ivan Cimrák

Received: 27 September 2007 / Accepted: 27 September 2007 / Published online: 8 May 2008

Abstract The Landau-Lifshitz (LL) equation of micromagnetism governs rich variety of the evolution of magnetization patterns in ferromagnetic media. This is due to the complexity of physical quantities appearing in the LL equation. This complexity causes also interesting mathematical properties of the LL equation: nonlocal character for some quantities, nonconvex side-constraints, strongly nonlinear terms. These effects influence also numerical approximations. In this work, recent developments on the approximation of weak solutions, together with the overview of well-known methods for strong solutions, are addressed.

1 Introduction

We aim at an exhaustive survey on recent advances in the numerics and computations of the problems coupled with the micromagnetic equation, also known as the Landau-Lifshitz equation of ferromagnetism. More general topic of recent developments in the modelling, analysis and numerics of ferromagnetism was discussed in a survey article [1]. However since then, many new ideas in numerics of micromagnetism appeared very recently and we feel necessary to address these improvements. Besides its importance in the modelling of ferromagnetic phenomena on micro- and nanoscales, the Landau-Lifshitz equation is interesting also from a mathematical point of view. Numerical analysis of several aspects such as sharp nonlinearity, transitions between different forms of the equation, and side-constraints, is very challenging.

In this survey, we focus on numerical methods dealing with various forms of the LL equation. We try to explain basic ideas of the schemes together with correct formulations in such a way that the reader gains an insight into the problems arising from the numerical approximation of the LL equation.

The text is organized as follows. In Sect. 1 (Introduction), we first present the micromagnetic model and list basic properties of the micromagnetic system. At the end of this section we provide several applications of the LL equation in both the theoretical physics and the real world applications in magnetic recording industry.

The main text is devoted to numerical schemes. According to the level of theoretical knowledge about the convergence behavior of the schemes, the text is split into two parts: In Sect. 2, we study numerical schemes for which no rigorous convergence analysis is known, and in Sect. 3, we consider those methods for which convergence results were successfully obtained.

Finally in Sect. 4, we show several computational studies presenting the behavior of selected schemes. The last example deals with adaptivity strategies for the LL equation.

1.1 Micromagnetism and Free Energy of Ferromagnetic Body

For magnetic materials, the relation between the magnetic field $\mathbf{H}$ and the magnetic induction $\mathbf{B}$ is expressed by $\mathbf{B} = \mu_0(\mathbf{H} + \mathbf{M})$, using the quantity *magnetization* denoted by $\mathbf{M}$. Magnetization is a property of materials that describes to what extent they are affected by magnetic fields, and also

Author is supported by the Fund for Scientific Research—Flanders FWO (Belgium).

I. Cimrák (✉)
Numerical and Functional Analysis and Mathematical Modeling Research Group NfaM², Department of Mathematical Analysis, Ghent University, Galglaan 2, 9000 Ghent, Belgium
e-mail: ivan.cimrak@ugent.be

determines the magnetic field that the material itself creates. Magnetization is defined as the amount of magnetic moment per unit volume. The origin of the magnetic moments creating the magnetization can be either microscopic electric currents corresponding to the motion of electrons in atoms, or the spin of the electrons.

In some materials (e.g., ferromagnets), the magnetization exists even without an external magnetic field (spontaneous magnetization). In other types of materials, the magnetization is induced when an external magnetic field only is present. The magnetization is not always homogeneous within a body, but rather a function of position.

For ferromagnetic materials at temperature far below the so called *Curie temperature* $\mathcal{T}_C$, the modulus of the magnetization remains constant. Thus one can presume

$$\mathbf{M} = M_s \mathbf{m}, \tag{1}$$

where $\mathbf{m}$ is a unit vector.

Micromagnetism deals with the interactions between magnetic moments on sub-micrometer length scales. These are governed by several competing energy terms. The total energy involved, called *free energy*, consist of several contributions describing different phenomena appearing in ferromagnetic bodies.

Exchange energy. Orientation of the magnetization vector can vary from point to point. Exchange energy will attempt to make the magnetic moments in the immediately surrounding space lie parallel to one another. Therefore it costs additional energy to change the direction of the magnetization. We call this the *exchange energy*. This energy can be measured by the gradient of $\mathbf{m}$ and its simplest approximation can be written as

$$\begin{aligned} E_{\text{exc}} &= \int A_{\text{exc}} \big[(\nabla \mathbf{m}_{x_1})^2 + (\nabla \mathbf{m}_{x_2})^2 + (\nabla \mathbf{m}_{x_3})^2 \big] \\ &= \int A_{\text{exc}} |\nabla \mathbf{m}|^2, \end{aligned} \tag{2}$$

where A_{exc} is a material constant, see [2].

Anisotropy energy. The properties of a magnetic material are in general dependent on the directions in which they are measured. In the absence of all external forces, the magnetization $\mathbf{M}$ would align in one or more specific directions in the crystal lattice. We call these directions *easy axes* of the material.

To rotate the magnetization away from the easy axis involves energy called *anisotropy energy*. For case of material with uniaxial anisotropy (one easy axis of magnetization is present, represented by vector $\mathbf{p}$) the anisotropy energy can be expressed as

$$E_{\text{ani}} = \int K_{\text{ani}} \langle \mathbf{m}, \mathbf{p} \rangle^2.$$

Zeeman's energy. The magnetic system can be influenced by an externally applied field. This type of field is called *applied field* and we denote it by $\mathbf{H}_{\text{app}}$. It interacts with the magnetization and creates an energy called *Zeeman's* or *applied field energy*. This energy contribution describes the tendency of the magnetization to align external applied field. It is given by

$$E_{\text{app}} = \int \mu_0 \langle \mathbf{H}_{\text{app}}, \mathbf{M} \rangle.$$

Magnetostatic energy. Magnetostatic interactions represent the way the elementary magnetic moments interact over long distances within the body. In fact, the magnetostatic field at a given location within the body depends on the contributions from the whole magnetization vector field. Magnetostatic interactions can be taken into account by introducing the appropriate magnetostatic field $\mathbf{H}_{\text{dem}}$ according to static Maxwell equations for magnetized media

$$\left.\begin{aligned} \nabla \cdot \mathbf{H}_{\text{dem}} &= -\nabla \cdot \chi_\Omega \mathbf{M} \\ \nabla \times \mathbf{H}_{\text{dem}} &= 0 \end{aligned}\right\} \quad \text{in } \mathbb{R}^n, \tag{3}$$

where χ_Ω is a characteristic function of the domain Ω occupied by ferromagnetic body. Then, the energy coupled with magnetostatic interactions denoted by E_{dem} will be expressed as

$$E_{\text{dem}} = \int \frac{1}{2} \mu_0 \langle \mathbf{H}_{\text{dem}}, \mathbf{M} \rangle.$$

Magnetostrictive energy. Materials in which reversible deformation can be induced by an applied magnetic field and in which applied stress results in a change of the magnetization are called magnetostrictive materials. The so called *magnetostrictive energy* linked to this behavior can be expressed in terms of *magnetostriction field* $\mathbf{H}_{\text{str}}$ defined according to tensor conventions as

$$\mathbf{H}_{\text{str}} = \lambda^m \sigma : \mathbf{M}, \tag{4}$$

where $\sigma = \sigma(\mathbf{u}, \mathbf{M})$ depends on the magnetization and the displacement vector $\mathbf{u}$ via the relation

$$\sigma = \lambda^\epsilon \epsilon(\mathbf{u}) - \lambda^\epsilon \lambda^m \mathbf{M}\mathbf{M}^T.$$

The strain tensor is defined as

$$\epsilon_{ij}(\mathbf{u}) = \frac{1}{2}(\partial_{x_j} u_i + \partial_{x_i} u_j).$$

Tensors $\lambda^\epsilon, \lambda^m$ describe the properties of the material. The displacement vector $\mathbf{u}$ and the stress tensor σ are coupled by the equation of elastodynamics

$$\rho \mathbf{u}_{tt} - \nabla \cdot \sigma = 0,$$

where ρ is the mass density. Thus the magnetostrictive energy can be expressed as

$$E_{\text{str}} = \int \frac{1}{2}\mu_0 \langle \mathbf{H}_{\text{str}}, \mathbf{M} \rangle.$$

Total free energy E_{free} of a ferromagnetic system can be then expressed as sum of all contributions listed above. Since the most efficient magnetic alignment (also known as a configuration) is the one in which the energy is lowest, these five energy terms will attempt to become as small as possible at the expense of the others, yielding complex physical interactions. The competition of these interactions under different conditions is responsible for the overall behavior of a magnetic system. The system will reach an equilibrium state when the configuration of the magnetization will correspond to some local minimizer of the energy functional $E_{\text{free}}(\mathbf{m})$.

1.2 Dynamics in a Ferromagnetic Body

Considering the case of a ferromagnetic body, we deal with a system whose free energy E_{free} has many local minima corresponding to metastable equilibria [2]. In this framework, one can determine the equilibrium condition by imposing that the free energy is stationary with respect to $\mathbf{M}$. It is important to underline that, from this analysis, one can not say which metastable state the system will reach, given an initial state. The only way to determine this information is to introduce dynamics. Therefore, an appropriate dynamic equation must be considered to describe the evolution of the system.

First, we have to understand that any system can only feel the magnetic field that results from an energy change. So we have to derive a total *effective field*, denoted by $\mathbf{H}_{\text{eff}}$, acting on the magnetization as derivative of the energy density function e_{free} for E_{free} defined by $E_{\text{free}} = \int e_{\text{free}}$. Eventually, the effective field takes form

$$\begin{aligned}\mathbf{H}_{\text{eff}} &= \mathbf{H}_{\text{exc}} + \mathbf{H}_{\text{ani}} + \mathbf{H}_{\text{app}} + \mathbf{H}_{\text{dem}} + \mathbf{H}_{\text{str}} \\ &= -\frac{\partial e_{\text{free}}}{\partial \mathbf{m}}, \end{aligned} \tag{5}$$

where $\mathbf{H}_{\text{exc}} = A_{\text{exc}} \Delta \mathbf{M}$ denotes *the exchange field* and $\mathbf{H}_{\text{ani}} = K_{\text{ani}} \langle \mathbf{m}, \mathbf{p} \rangle \mathbf{p}$ stands for *the anisotropy field*. The other symbols were explained before.

The first dynamical model for the precessional motion of the magnetization was proposed by Landau and Lifshitz in 1935 [3]. Basically, this model includes two types of precession, rotational and dissipative. Rotational precession describes the rotation of the magnetization vector around the vector of the effective field. This movement perfectly matches the theory of gyromagnetic precession, however it is a conservative process. For modelling of real processes, which are in their nature dissipative, a phenomenological term was introduced to describe the dissipation of the energy by pushing $\mathbf{M}$ towards $\mathbf{H}_{\text{eff}}$.

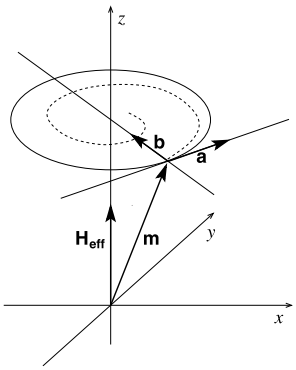

Fig. 1 The combination of precessional and dissipative movement of $\mathbf{m}$ around $\mathbf{H}_{\text{eff}}$. The component denoted as $\mathbf{b}$ represents the term $-\mathbf{m} \times (\mathbf{m} \times \mathbf{H}_{\text{eff}})$ while $\mathbf{a}$ stands for the component $-\mathbf{m} \times \mathbf{H}_{\text{eff}}$

The combination of two movements is governed by the so called *Landau-Lifshitz* (LL) equation

$$\mathbf{m}_t = -\beta_L \mathbf{m} \times \mathbf{H}_{\text{eff}} - \alpha_L \mathbf{m} \times (\mathbf{m} \times \mathbf{H}_{\text{eff}}). \tag{6}$$

We often refer to (6) as the Landau-Lifshitz form (or shortly the LL form) of the micromagnetic equation.

Remark 1 The complete physical model encounters the following physical constants and parameters: γ the gyromagnetic ratio, α the damping parameter and M_s the saturation magnetization. The Landau-Lifshitz equation then reads as

$$\mathbf{M}_t = -\gamma \left(\mathbf{M} \times \mathbf{H}_{\text{eff}} + \alpha \frac{\mathbf{M}}{M_s} \times (\mathbf{M} \times \mathbf{H}_{\text{eff}}) \right). \tag{7}$$

However, for the purposes of mathematical analysis it is more suitable to distinguish between the coefficients in front of the terms in the equation separately. Therefore we use α_L and β_L related to physical constants by $\beta_L = \gamma$ and $\alpha_L = \alpha\gamma$. Moreover we work with normalized magnetization $\mathbf{m}$ and thus the time is scaled by a factor M_s^{-1}.

The length of $\mathbf{m}$ does not change during the evolution process described by the LL equation. The reader can check this statement by scalar multiplication of (6) with $\mathbf{m}$.

In Fig. 1 both terms appearing on the r.h.s. of (6) are illustrated. The dissipative character represented by the second term on the r.h.s. of (6) is characterized by condition $\alpha_L > 0$.

It is not always necessary to include all contributions to the effective field in (5). For example, when one does not expect large deformations of the working sample, the magnetostrictive part can be neglected. Or, in the case of uniformly magnetized bodies, it is the exchange field that vanishes.

The mathematical properties of the LL equation are given by the actual form of $\mathbf{H}_{\text{eff}}$. They vary significantly when only some terms in (5) are considered. The contributions can be divided according three main ingredients influencing actual type of the LL equation.

1. Anisotropy—direct dependence on values of $\mathbf{m}$. Including the anisotropy field makes the LL equation an ODE.
2. Exchange—direct dependence on gradient of $\mathbf{m}$. Including the exchange field makes the LL equation a PDE.
3. Magnetostatics and magnetostriction—indirect dependence on $\mathbf{m}$ or $\nabla\mathbf{m}$ via an additional PDE. Including the magnetostatic and the magnetostrictive field requires another PDE to be coupled with the LL equation.

Also computational aspects are affected by the choice of terms contributing to the effective field. We should distinguish between two major cases.

Local interactions. Energy terms including exchange, anisotropy and Zeeman's energy describe local (in space) interactions. It means that local change of the magnetization affects corresponding field only locally. Therefore, e.g. during the assembling of the mass matrix one can consider values only on the neighboring vertexes of the mesh.

Long-distance interactions. On the other side, the magnetostatic and magnetostrictive energy characterize long distance interactions. As an example, the local change of the magnetization changes locally the r.h.s. of (3). This however results in the global change of $\mathbf{H}_{\text{dem}}$. The same can be said also for the magnetostrictive contribution. For computations makes this quite a problem, mainly on the amount of the computations.

A different approach for description of damped precession was proposed by Gilbert [4]. He introduced the following equation

$$\mathbf{m}_t - \alpha_G \mathbf{m} \times \mathbf{m}_t = -\beta_G \mathbf{m} \times \mathbf{H}_{\text{eff}}, \tag{8}$$

which was later named as the *Landau-Lifshitz-Gilbert* (LLG) equation. Here, the damping is incorporated implicitly as the precession direction is no longer perpendicular to $\mathbf{H}_{\text{eff}}$.

We refer often to (8) as the Landau-Lifshitz-Gilbert form of the micromagnetic equation (LLG form).

Although the previous equation seems to be different from the LL form, it can be proved that for $\beta_L \neq 0$ they are mathematically equivalent. To see this, compute the cross product of (6) with $\mathbf{m}$ to get

$$\mathbf{m} \times \mathbf{m}_t = -\beta_L \mathbf{m} \times (\mathbf{m} \times \mathbf{H}_{\text{eff}}) - \alpha_L \mathbf{m} \times (\mathbf{m} \times (\mathbf{m} \times \mathbf{H}_{\text{eff}})).$$

Using the identity $\mathbf{m} \times \mathbf{H}_{\text{eff}} = -\mathbf{m} \times (\mathbf{m} \times (\mathbf{m} \times \mathbf{H}_{\text{eff}}))$, which holds true once $|\mathbf{m}| = 1$, we get

$$-\frac{\alpha_L}{\beta_L}\mathbf{m} \times \mathbf{m}_t = \alpha_L \mathbf{m} \times (\mathbf{m} \times \mathbf{H}_{\text{eff}}) - \frac{\alpha_L^2}{\beta_L}\mathbf{m} \times \mathbf{H}_{\text{eff}}.$$

Summing up the previous equation with (6) leads to the LLG form with coefficient transformation

$$\alpha_G = \frac{\alpha_L}{\beta_L} \quad \text{and} \quad \beta_G = \frac{\alpha_L^2 + \beta_L^2}{\beta_L}.$$

Remark 2 Although the LL and the LLG forms are for $\beta_L \neq 0$ mathematically equivalent and give the same solutions, for numerics it makes difference. The schemes derived from the LL form using, e.g., backward Euler approximation of time derivative, can behave differently from those derived from the LLG form. As an example, compare Algorithm 2 of Prohl and Bartels described in Sect. 3.4, which is based on the LLG form, with Algorithm 7, which is based on the LL form.

Remark 3 Comparing the LL form with the LLG form, we can conclude that the LLG form is in general more suitable for numerical schemes than the LL form. The reason for this is that without the double cross term, the LLG form can drastically simplify the treatment of damping in the algorithm. One could object that the LL form has the advantage of explicitly expressed time derivative of $\mathbf{m}$. However, since the mid-point scheme is already implicit, the implicit nature of the LLG form does not introduce any further complication.

We go further and derive another form of the micromagnetic equation different from the LL and the LLG form. Using the similar calculus as before we end up with

$$\mathbf{m}_t + \alpha_C \mathbf{m} \times \mathbf{m}_t = -\beta_C \mathbf{m} \times (\mathbf{m} \times \mathbf{H}_{\text{eff}}), \tag{9}$$

where $\alpha_C = \alpha_G^{-1} = \beta_L/\alpha_L$ and $\beta_C = \beta_G \alpha_G^{-1} = (\alpha_L^2 + \beta_L^2)/\alpha_L$.

1.3 Basic Properties of the Micromagnetic System

It is a classical dilemma: Which approach to use in the computations. Which numerical scheme should be implemented in order to get the best results? There are several approaches. The method of "rude force" suggests to take the explicit Euler method with tiny time-steps in order to get the truncation error minimal. With a cleverer approach—however sometimes not so efficient—we would use the highest order scheme which can be computed with our computational facilities in a reasonable time. Both can eventually suffer from numerical instabilities and from non-physical results.

Possible solution is to use such a numerical scheme that follows physical properties of the system under consideration. The previous two approaches were just general schemes and thus it would be naive to expect the best results.

Let us list the most important physical features of the LL system, proposed in [5], that can be taken under consideration when developing a numerical scheme.

Conservation of the modulus. From (1) we see that the length of the magnetization is conserved in time at each spatial location. It is a fundamental constraint on the evolution of the magnetization that should be respected in the time discretized version of the LL equation. Classic schemes, like the backward Euler scheme, do not preserve this feature. For some schemes, once the error estimates are derived, also an asymptotic conservation of the length of the magnetization can be verified, when the time-stepping goes to zero [6, 7].

Other schemes are designed in such a way that the solution is projected back on the sphere in every time step or after a prescribed tolerance has been exceeded. This is a nonlinear modification of the original LLG dynamics which may cause troubles in the analysis of the scheme.

The third approach is to use a numerical scheme preserving the length of the magnetization directly. A family of such schemes use so called *mid-point rule*. We mention several examples in Sects. 2 and 3.

Liapounov structure. As mentioned already in [8], in case of constant applied field the LL equation has so called *Liapounov structure*, i.e., the free energy of the system is a nonincreasing function of time. This can be derived from scalar multiplication of (6) by $\mathbf{H}_{\text{eff}}$ and integration over the domain

$$-(\mathbf{m}_t, \mathbf{H}_{\text{eff}}) + \alpha_L \|\mathbf{m} \times \mathbf{H}_{\text{eff}}\|_2^2 = 0.$$

From (5) we have

$$(\mathbf{m}_t, \mathbf{H}_{\text{eff}}) = \left(\mathbf{m}_t, -\frac{\partial e_{\text{free}}}{\partial \mathbf{m}}\right) = -\int \frac{\partial e_{\text{free}}}{\partial t} = -\frac{\partial E_{\text{free}}}{\partial t},$$

which after time integration leads to the verification of the Liapounov structure of the LL equation.

This property is also fundamental, because it guarantees that the system tends toward stable equilibrium points, which are minima of the free energy. It is thus natural to demand that the time discretization preserves the Liapounov structure.

Hamiltonian structure. Third property mentioned in [5] emphasize the fact that the LL equation was derived originally from a Hamiltonian system, which is conservative with respect to the energy. The addition of the phenomenological damping term introduces the possibility to describe real systems featuring dissipative mechanisms. However, in many applications, the damping effects can be considered as a perturbation of the conservative motion, since the ratio $\frac{\alpha_L}{\beta_L}$ varies around 0.02. In this respect, the third important property of the LL equation is the Hamiltonian structure when $\alpha_L = 0$.

Remark 4 Until now, the mid-point rule based numerical schemes were very effective, however, for the case of exchange field included in the model, without a rigorous justification. Only so called *asymptotic analysis* argumentation was used in order to determine the accuracy of the method. This argumentation relies on the approximations of respective terms using expressions with certain order of accuracy. This approach however does not serve for rigorous error estimates or at least convergence analysis of the scheme. It is not straightforward that if respective terms in a PDE are approximated with some order of accuracy then the solutions of the approximate PDE will actually converge (with the same of in some cases lower order) to the solution of original PDE.

Very recent results of Bartels and Prohl however show that it is possible to analyze the mid-point rule based schemes rigorously.

1.4 Applications

We show several areas where the Landau-Lifshitz equation plays a key role in an accurate description of the magnetic processes.

1.4.1 Maxwell-LLG Model

To obtain a simple model problem for ferromagnetic calculations, we suppose that there is a bounded cavity $\Omega^{\text{out}} \subset \mathbb{R}^3$ with perfectly conducting outer surface Γ^{out}. Within the cavity is a ferromagnetic material occupying a bounded subdomain $\Omega \subset \Omega^{\text{out}}$. For simplicity we assume that outside the ferromagnet is vacuum.

In order to model the electromagnetic behavior of the ferromagnetic material, the basic Maxwell system must be augmented by the Landau-Lifshitz equation describing the influence of the ferromagnet. The electromagnetic field in Ω^{out} is described by four vector functions of position and time: **E** the electric field, **H** the magnetic field, **B** the magnetic induction and **M** the magnetization. The magnetic variables are related as follows:

$$\mathbf{B} = \mu_0(\mathbf{H} + \mathbf{m}) \quad \text{in } \Omega^{\text{out}},$$

where $\mu_0 \geq 0$ is the magnetic permeability of free space. Replacing the variable **B** in standard Maxwell equations we arrive at the complete coupled Maxwell-Landau-Lifshitz (M-LL) system

$$\mathbf{m}_t + \alpha \mathbf{m} \times \mathbf{m}_t = (1+\alpha^2)\mathbf{m} \times \mathbf{H}_{\text{eff}} \quad \text{in } \Omega_T := (0,T) \times \Omega, \tag{10}$$

$$\varepsilon_0 \mathbf{E}_t + \nabla \times \mathbf{H} + \sigma \chi_\Omega \mathbf{E} = -\mathbf{J} \quad \text{in } \Omega_T^{\text{out}} := (0,T) \times \Omega^{\text{out}}, \tag{11}$$

$$\mu_0 \mathbf{H}_t - \nabla \times \mathbf{E} = -\mu_0 \mathbf{m}_t \quad \text{in } \Omega_T^{\text{out}}, \tag{12}$$

where $\beta_L = -1$ and $\alpha_L = \alpha$. Simplified effective field $\mathbf{H}_{\text{eff}} = \Delta\mathbf{m} + \mathbf{H}$ comprises main difficulties of the general version, where more terms contributing to the effective field are taken in consideration, see Sect. 1.1. The magnetic field $\mathbf{H}$ corresponds to the magnetostatic field $\mathbf{H}_{\text{dem}}$ of the micromagnetic system. Further, $\varepsilon_0 \geq 0$ denotes the electric permeability of free space, and $\sigma \geq 0$ the conductivity. Let $\mathbf{J} : \Omega_T^{\text{out}} \to \mathbb{R}^3$ denote the applied current density, and $\chi_\Omega : \Omega^{\text{out}} \to \{0, 1\}$ the characteristic function of Ω. System (10)–(12) is supplemented with initial conditions,

$$\mathbf{m}(0, \cdot) = \mathbf{m}_0 \quad \text{in } \Omega,$$
$$\mathbf{E}(0.\cdot) = \mathbf{E}_0, \quad \mathbf{H}(0, \cdot) = \mathbf{H}_0 \quad \text{in } \Omega^{\text{out}},$$

and boundary conditions,

$$\partial_{\mathbf{n}}\mathbf{m} = 0 \quad \text{on } \partial\Omega_T, \qquad \mathbf{E} \times \mathbf{n} = 0 \quad \text{on } \Omega_T^{\text{out}}.$$

In [9], stability of a semidiscrete scheme to numerically solve (10)–(12) is verified, but its convergence was not studied. Recently, Baňas, Bartels and Prohl [10] propose an implicit discretization of (10)–(12) and they succeed to prove the convergence. We focus on this topic in Sect. 3.7.

1.4.2 Magnetic Recording

The development of new magnetic materials used for permanent magnets, data storage, or magnetic sensors asks for realistic simulation of modern magnetic materials. Thus one needs to make accurate predictions of their magnetic properties. The LL model describes magnetic phenomena on submicron scales, thus it is well suited for the modelling. Moreover, advanced numerical micromagnetic simulations justified the ability to provide theoretical guidelines for the structural design of novel magnetic materials and devices.

The following topics employ the LL formalism in the description and simulations.

Discrete storage media comprise huge potential for future advances in ultra-high density magnetic recording.

Perpendicular magnetic recording is a candidate to deal with thermal instabilities in conventional longitudinal recording.

Magnetic nano-wires. New developments of magneto-electronic devices may be based on the magnetoresistance of domain walls moving in nano-wires.

Vortexes in nano-elements. The applications in sensors are very sensitive for switching behavior and for the creation of so called *vortexes*. Therefore a fine analysis of the behavior of such vortexes is of great interest. Recently, a novel numerical scheme has been developed by Bartels and Prohl [11] capable to trace the behavior of the vortexes very accurate. The authors prove also the convergence of this scheme, which is described later in Sect. 3.4.

1.4.3 Thermally Activated Micromagnetics

Thermally activated processes become increasingly important in magnetic recording and sensor applications. Thermal stability and fast writing are crucial for ultra high density magnetic recording. With decreasing bit size, thermal effects are relevant to high speed switching of the magnetization in the write process and to the long term stability of the written bit.

There exist more ways how to treat thermally activated processes. We mention two of them: First way is to incorporate a stochastic thermal field $\mathbf{H}_{\text{thm}}$ to the effective field $\mathbf{H}_{\text{eff}}$. Second way is to consider non-constant length of magnetization M_s introduced by (1).

Stochastic thermal field $\mathbf{H}_{\text{thm}}$. Inclusion of a stochastic process in the effective field accounts for the interaction of the magnetic polarization with the microscopic degrees of freedom. This interaction causes the fluctuation of the magnetization distribution. This approach was originally introduced by Brown [12] for a single domain particle with uniform magnetization.

The thermal field is assumed to be a random process with the property that the average of $\mathbf{H}_{\text{thm}}$ taken over different realizations vanishes in each direction of space, thus $\langle \mathbf{H}^i_{\text{thm}}(t) \rangle = 0$. This is so because a large number of microscopic degrees of freedom contribute to this mechanism.

Further, due to the fluctuation-dissipation theorem [13] the strength of the thermal fluctuations denoted by D is related to the dissipation via the damping of the system by $D = \frac{\alpha_G k_B T}{\beta_G V}$, where T is the temperature, k_B is the so called *Boltzmann constant* and V denotes the spatial correlation length of the random field. Usually, V is taken to be equal to the cell size of the computational grid. However, recent results from [14] suggest that the calculated properties of the system are independent of the cell size if the cell size is smaller than the thermal exchange length $(A_{\text{exc}}/M_s|\mathbf{H}_{\text{thm}}|)^{1/2}$.

Further, the thermal field obeys

$$\langle \mathbf{H}^i_{\text{thm}}(t_1)\mathbf{H}^j_{\text{thm}}(t_2) \rangle = 2D\delta_{ij}\delta(t_1 - t_2).$$

The Kronecker δ_{ij} expresses the property of $\mathbf{H}_{\text{thm}}$ that its different components in space are uncorrelated, and the Dirac δ expresses that the autocorrelation time of the thermal field is much shorter than the response time of the system.

Finally, after adding $\mathbf{H}_{\text{thm}}$ to the total effective field in the LL equation and rearranging and regrouping deterministic and stochastic terms, we end up with the following system of Langevin equations

$$\mathbf{m}_t = \mathcal{A}(\mathbf{m}, t) + \mathcal{B}(\mathbf{m}, t)\mathbf{H}_{\text{thm}}(t).$$

It is a general system with multiplicative noise, since the multiplicative factor $\mathcal{B}$ for the stochastic process $\mathbf{H}_{\text{thm}}$ is a function of $\mathbf{m}$.

A stochastic process representing the fluctuating field is assumed to be Gaussian white noise, because the fluctuations emerge from the interaction of the magnetization with a large number of independent microscopic degrees of freedom with equivalent stochastic properties. As a result of the central limit theorem, the fluctuation field is Gaussian distributed.

In the calculus of stochastic differential equations (SDE) there exist two different interpretations of actual SDE called *Itô interpretation* and *Stratonovich interpretation.* Garcia-Palacios and Lazaro [15] proved that the equation has to be interpreted in the sense of Stratonovich, in order to obtain the correct thermal equilibrium properties.

For the stochastic computations standard stochastic calculus can be used, e.g. Euler-Maruyama method, which is only a straightforward generalization of the deterministic Euler method, or Heun method, which is a predictor-corrector based method. It turns out, that the Heun method fits better since it naturally converges to the solution of SDE in Stratonovich sense [16]. Recently, Monte Carlo based methods were used for stochastic computations for LLG including the thermal field [17].

Non-constant length of the magnetization. Thermomagnetic recording uses local heating of ferromagnetic media to locally decrease coercivity and change saturation magnetization M_s of the material and alleviate magnetization reversal. The long-term thermal stability of data/magnetic regions depends on material properties like saturation magnetization M_s and uniaxial magnetocrystalline anisotropy K_{ani}. The magnitude of both monotonically drops towards zero as the material temperature $\mathcal{T}$ is increased toward the Curie temperature $\mathcal{T}_C$. For $\mathcal{T}$ close to $\mathcal{T}_C$, thermal energy overcomes electronic exchange forces in ferromagnets and produces a randomizing effect, leading to total disorder, and hence zero length of the magnetization M_s.

The modelling of above mentioned thermomagnetic processes requires a model encountering the change of M_s during the magnetic reversal. An promising idea is proposed by Baňas, Prohl and Slodička in [18]. They suggest to consider an extended Landau-Lifshitz equation allowing for changes in the saturation magnetization. The subsequent modified Landau-Lifshitz model uses mutual orthogonality of $\mathbf{m}$, $\mathbf{m}\times\mathbf{H}_{\text{eff}}$ and $\mathbf{m}\times(\mathbf{m}\times\mathbf{H}_{\text{eff}})$ to describe temperature dependent gyroscopic precession. The model reads as

$$\mathbf{m}_t = \kappa\mathbf{m} - \beta_L\mathbf{m}\times\mathbf{H}_{\text{eff}} - \alpha_L\frac{\mathbf{m}}{M_s}\times(\mathbf{m}\times\mathbf{H}_{\text{eff}}) \quad \text{in } \Omega_T, \tag{13}$$

$$\partial_{\mathbf{n}}\mathbf{m} = 0 \quad \text{on } \partial\Omega_T, \tag{14}$$

$$\mathbf{m}(0,\cdot) = \mathbf{m}_0. \tag{15}$$

The function κ is chosen in such a way that M_s evolves according to the experimental values. Once M_s is known—from experiments or from e.g. mean field theory—actual determination of κ can be done from scalar multiplication of (13) by $\mathbf{m}$ resulting in

$$M_{s_t}^2 = 2\kappa M_s^2.$$

In classical form of the LL equation (6), the length of $\mathbf{m}$ is conserved. Analytical studies regarding the existence and regularity of the solutions rely on this fact. In the present case, the target for solutions of (13)–(15) depends on $(t,\mathbf{x})\in\Omega_T$ which is an innovative approach. In [18], the authors verify existence of locally strong and globally weak solutions, for $\Omega\subset\mathbb{R}^d$, $d=2,3$ being a bounded Lipschitz domain. More precisely, the first result uses abstract results, where locally strong solutions are constructed as proper limits of a sequence of smooth solutions. The existence of such smooth solutions follows from general inverse function theorem. The second result describes the construction of weak solutions as proper limits of iterates of a practical discretization in space-time.

From a numerical viewpoint, to construct convergent, fully practical numerical schemes where iterates respect the constraint $|m| = M_s > 0$ in a proper sense is a nontrivial endeavor. Over the last decade, projection strategies have been shown to converge in the context of (locally existing) strong solutions for the LL equation, where $M_s \equiv const$, and optimal convergence rates have been verified in this case [6]. Unfortunately, convergence of these methods in the case of only weak solutions is still not clear. It is only recently that space-time discretizations of the LL equation for $M_s \equiv const$ were found, where first iterates satisfy $|\mathbf{M}^j| = const$ at all nodes of the triangulation being j index of the temporal discretization, and second, the iterates construct weak solutions in the limit when all discretization parameters tend to zero. Interestingly, both ansatzes use different formulations of the problem in the continuous setting, leading to different schemes, numerical analysis, and properties as indicated.

The case of $0 < M_s \equiv M_s(t,\mathbf{x})$ makes the construction of stable, convergent discretizations, which satisfy $|\mathbf{M}^j| = M_s > 0$ even only at mesh-points challenging. Authors from [18] present two discretizations of (13)–(15), which are also based on two different formulations: first formulation uses the relation (20) and the second formulation departs from the LLG form (8) and uses the idea of cross-product type schemes described in Sects. 3.4–3.6.

1.4.4 Sensitivity Analysis of the LL Equation

The Landau-Lifshitz model is a complex model describing wide variety of physical quantities and properties of the medium. There are plenty constants, parameter functions

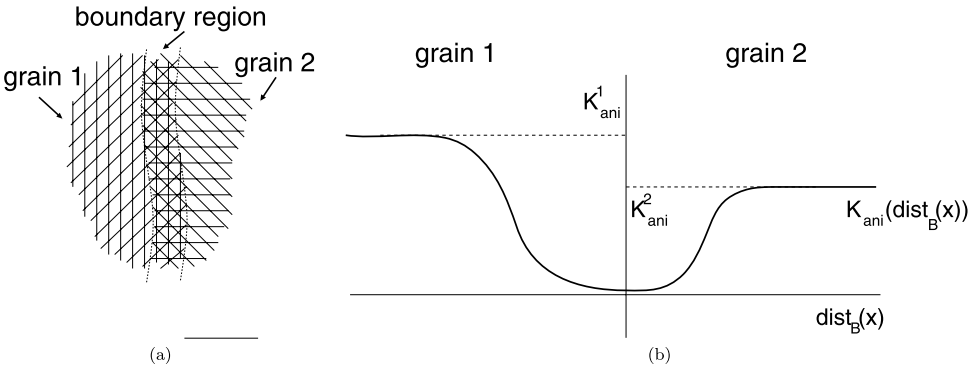

Fig. 2 (**a**) Schematic model of molecular lattice of two grains. In the boundary region the regularity of the lattice vanishes which results in the drop of the anisotropy parameter K_{ani}. (**b**) The profile of K_{ani} having value K^1_{ani} inside grain 1, having value close to zero in the boundary region and again rising to value K^2_{ani} inside grain 2

and coefficients appearing in the model determined by a particular problem. Some constants are the same and are known in all cases, e.g. gyromagnetic factor γ. However, most parameters change from case to case. For some systems the values of these parameters are known in forehand but many times they have to be determined by an experiment. For example, the anisotropy constant was measured already for many materials. However, as soon as you deal with nonuniform materials, e.g. composites, the actual values can differ from the values found in the books.

The determination of the parameters of PDE's is a complicated task and it is in general an inverse problem. That means that from the measurements of the state variable, e.g. the magnetization or the magnetic field, one has to determine the parameters of the PDE. Inverse problems are in general ill-posed and the solution is highly sensitive on the data. Therefore, a careful analysis of the sensitivity of the LL equation on the parameters has to be performed in order to design the algorithms for parameter identification.

The so called *sensitivity analysis* mentioned above, is important also to optimization problems. In this sort of problems one has to find optimal value of some parameters in order to minimize in forehand known functional. The optimization procedure often requires knowledge of how sensitive the solution is to the change of some parameters.

We will provide several examples.

Non-constant anisotropy parameter. In the high-density magnetic recording, so called *grained media* are used. The material consists of many grains. Every grain features an uniform anisotropy, i.e. the anisotropy parameter K_{ani} is known over every grain. The problem arises in region where two grains touche. More specifically, going from the middle of one grain towards the boundary with another grain, the value of anisotropy parameter drops almost to zero. When passing the boundary and moving towards the middle of another grain, anisotropy parameter again rises. This is due to the crystalline structure of material: Anisotropy is connected with the regularity of molecular lattice. When going from one grain to another, this regularity is broken (see Fig. 2a) and therefore the value of anisotropy parameter drops and rises.

For accurate modelling of magnetic recording it is desirable to know exact profile of this drop-and-rise function. When we denote $\text{dist}_B(\mathbf{x})$ a space variable function measuring the distance of $\mathbf{x}$ to the nearest boundary of the current grain, the anisotropy parameter K_{ani} becomes space dependent function

$$K_{\text{ani}} = K_{\text{ani}}(\text{dist}_B(\mathbf{x})),$$

having the graph similar as depicted in Fig. 2b. However, the exact shape of $K_{\text{ani}}(\text{dist}_B(\mathbf{x}))$ can not be measured directly since the current techniques are not capable of measuring anisotropy of molecular lattice on such small scales. Therefore the inverse problem has to come into play and the shape of $K_{\text{ani}}(\text{dist}_B(\mathbf{x}))$ is determined indirectly from the measurements of magnetic field around the boundary.

Non-constant damping parameter. For a composite materials, the damping constant α can be a space dependent function. This phenomenon results from the fact that there are regions where the density of the particles from one material is higher than in other places. This is difficult to capture by standard methods and must be again determined indirectly from measurements of magnetic field.

Shape optimization of the working domain. In recording industry, the efficiency of writing data onto thin films is significantly influenced by the actual shape of the writing head. The writing process can be described by the Landau-Lifshitz formalism where the part of the working domain is the head self. For the optimal writing and reading one has to find the optimal shape of the writing head. Thus the parameters describing the shape of the head are to be determined from the optimization process.

Core optimization in MRAM-type memories. New advances in nanotechnologies gives a good hope that the *Magnetoresistive Random Access Memories* will become competitive alternative to existing solutions like Flash RAM or DRAM. One of the approaches leading to better properties of MRAM is the design of the ferromagnetic core in one cell.

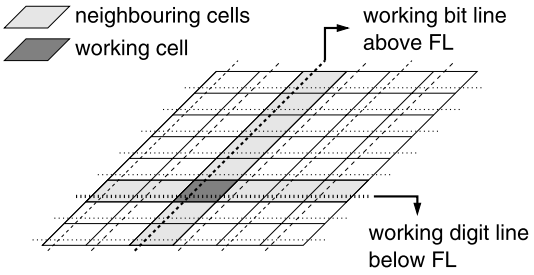

Fig. 3 Schematic model of MRAM. Writing in the working cell affects the information written in the neighboring cells along the working *bit line* and *digit line*

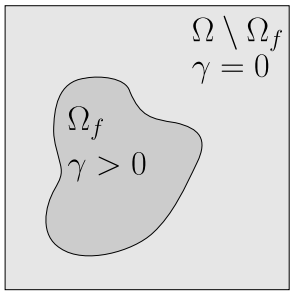

Fig. 4 Single cell occupying domain Ω. Area Ω_f characterized by $\gamma > 0$ describes shape of the core

Very simplified model of MRAM is depicted in Fig. 3. A ferromagnetic layer (FL) is divided in a grid of cells. Each cell is capable to hold a bit information 0 or 1 by magnetizing the core of the cell in one of two possible directions. Above the FL a grid of wires called *bit lines* is placed. Similarly, below the FL occurs a perpendicular grid of wires called *digit lines*. Writing of one bit in a particular working cell is done in the following way. Electric current passes through the digit line and the bit line located above and below the working cell, see Fig. 3. The current induces a field that changes the magnetization of the working cell to the final state representing written bit.

However, induced field acts also on the other cells located along the working bit line and digit line. Thus this phenomenon must be included in the shape optimization design.

One single cell occupying domain Ω consists of two parts. The core Ω_f is made of a ferromagnetic material and the rest of the cell denoted by $\Omega \setminus \Omega_f$ is made of nonmagnetic material separating cells from each other, see Fig. 4. The main aim of this work is to optimize the shape of Ω_f.

For the description of the dynamics during writing process the LL equation (6) can be used where $\alpha_L(\mathbf{x}) = C\beta_L(\mathbf{x})$ and moreover we allow α_L to be a space dependent function. The reason for this is to flexible describe the shape of magnetic core in MRAM. Notice that if $\alpha_L = 0$ then the LL equation reduces to trivial $\mathbf{m}_t = 0$, which means that $\mathbf{m}$ does not change in the part of the domain where $\alpha_L = 0$. On the other side, in the part of Ω where α_L is positive, we obtain classical LL equation, see Fig. 4. Of course, it would be ideal if α_L is a two-valued function having value 0 on $\Omega \setminus \Omega_f$ and having a constant value α_L^{const} on Ω_f. However we accept a continuous function α_L and later we try to force it to be an approximation of a two-valued function. Thus in this case, α_L is the parameter function that has to be optimized in order to get the best writing properties.

General Framework for Sensitivity Analysis

We describe a general framework used for optimization and inverse problems in micromagnetics.

We begin with notations. Model based on the LL equation in quite general form reads as

$$\mathcal{LL}(\mathbf{m}, \mathcal{P}) = 0, \tag{16}$$

equipped with corresponding initial and boundary conditions which we do not specify here. The expression $\mathcal{LL}$ depends on parameter (or set of parameters) $\mathcal{P}$ and on state variable $\mathbf{m}$ which is also dependant on $\mathcal{P}$. The relation (16) consists of the LL equation, possibly coupled with other equations such as magnetoelastic equation or Maxwell's equations.

Dependence of $\mathbf{m}$ on $\mathcal{P}$ is due to the fact that $\mathbf{m}$ is a solution of (16), so knowing the value $\mathcal{P}$ we are able to compute $\mathbf{m}(\mathcal{P})$ from (16).

Let us consider the following abstract problem.

Problem 1 Find a set of parameters $\mathcal{P}^*$ form a suitable space $\mathcal{Q}$, which minimizes a cost functional $\mathcal{F}(\mathbf{m})$, i.e,

$$\mathcal{P}^* = \operatorname*{argmin}_{\mathcal{P}\in\mathcal{Q}} \mathcal{F}(\mathbf{m}),$$

where $\mathcal{P}^*$ are parameters in the LL equation (16).

Concrete definitions of $\mathcal{Q}$ and $\mathcal{F}$ characterize the particular optimization or inverse problem. Typically, the cost functional $\mathcal{F}$ is written in terms of $\mathbf{m} = \mathbf{m}(\mathcal{P})$ as the solution to the LL equation with corresponding parameter set $\mathcal{P}$. In the case of inverse problems, $\mathcal{F}$ can express e.g. the difference between the computed solution $\mathbf{m}(\mathcal{P})$ and the measurements.

Many iterative minimization strategies, such as Steepest Descend Method or Newton-like methods, require knowledge of the derivative of $\mathcal{F}(\mathbf{m})$ with respect to $\mathcal{P}$ in every step of their iterations.

The working scheme can be as follows.

1. The differentiation of $\mathcal{F}(\mathbf{m})$ leads to

$$\frac{\partial \mathcal{F}(\mathbf{m})}{\partial \mathcal{P}} = \frac{\partial \mathcal{F}(\mathbf{m})}{\partial \mathbf{m}} \frac{\partial \mathbf{m}}{\partial \mathcal{P}}, \tag{17}$$

which means we have to find the derivation of $\mathbf{m}(\mathcal{P})$ with respect to $\mathcal{P}$.

2. The total differentiation of (16) gives the following equation for $\mathbf{m}$

$$D\mathcal{LL}(\mathbf{m},\mathcal{P}) = \frac{\partial \mathcal{LL}(\mathbf{m},\mathcal{P})}{\partial \mathbf{m}} \frac{\partial \mathbf{m}}{\partial \mathcal{P}} + \frac{\partial \mathcal{LL}(\mathbf{m},\mathcal{P})}{\partial \mathcal{P}} = 0 \tag{18}$$

   equipped with adapted initial and boundary conditions. So the solution of (18) gives us $\frac{\partial \mathbf{m}}{\partial \mathcal{P}}$.
3. Knowing $\frac{\partial \mathbf{m}}{\partial \mathcal{P}}$ one can perform one step in the iterative minimization procedure.

We present an example of the application of general framework described above. The example deals with the shape optimization of magnetic core in MRAM memories, mentioned already before in this section. It is one part of the work [19] where the authors consider the case when $\alpha_L(\mathbf{x}) = C\beta_L(\mathbf{x})$ and the set of parameters is $\mathcal{P} = \alpha_L$. They derived the expression for the Gâteaux derivative of $\mathcal{F}$ with respect to α_L using the primal-dual approach. Together with existence and uniqueness results for the Gâteaux derivative it creates the first application of sensitivity analysis of the LL equation. Further extension of this work can be found in [20].

Example 1 (Shape optimization of MRAM) We discuss the simplified model of MRAM mentioned before in this section. Let us continue in the description of the writing process. *Writing process* consists of a switching process when overall magnetization of the core is switched by an external magnetic field to the different direction. Three types of applied field occurs during the writing: $\mathbf{H}^{45}_{\text{app}}$ is induced by both the digit and the bit lines above the working cell, and $\mathbf{H}^{0}_{\text{app}}, \mathbf{H}^{90}_{\text{app}}$ are induced by just one of the digit or the bit line above the neighboring cells. One has to take care that $\mathbf{H}^{45}_{\text{app}}$ actually switches the direction of the magnetization in the working cell, while the influence of the fields $\mathbf{H}^{0}_{\text{app}}, \mathbf{H}^{90}_{\text{app}}$ on the neighboring cells will be minimal.

The construction of the cost functional mentioned in the definition of Problem 1 will follow the latter reasoning. We distinguish 2 different phenomena.

Quality of writing process. Data must be written correctly, so that after the writing process it is clear if 0 or 1 is written. This will be achieved by controlling that the average magnetization of the core is aligned with the direction of written bit. Consequently, if e.g. bit 1, represented by direction $\mathbf{p}_1$, should be written then, during the writing process, the change of $\mathbf{m}$ in the direction of $\mathbf{p}_1$ should be maximal. Therefore we aim at maximizing the quantity

$$\mathcal{F}_1 = \int_0^T \langle \mathbf{m}_t{}^{45}, \mathbf{p}_1 \rangle.$$

The superscript 45 indicates, that $\mathbf{m}^{45}$ is computed from the LL equation when $\mathbf{H}^{45}_{\text{app}}$ is in the play. Normally, directions $\mathbf{p}_1$ and $\mathbf{p}_2$ for bits 0 and 1 are the following ones $\mathbf{p}_1 = 2^{-\frac{1}{2}}(1,1,0)$ and $\mathbf{p}_2 = 2^{-\frac{1}{2}}(-1,1,0)$.

Influence on neighboring cells. Of course, writing process in the working cell can not influence the neighboring cells much. Thus the overall change of the magnetization in the neighboring cells must be minimal. This can be controlled by minimizing

$$\mathcal{F}_2 = \int_0^T \|\mathbf{m}_t{}^{\phi}\|_2^2,$$

where $\phi \in \{0, 90\}$ indicates that $\mathbf{m}$ is computed from the LL equation considering just one of $\mathbf{H}^{0}_{\text{app}}, \mathbf{H}^{90}_{\text{app}}$.

Notice that $\mathcal{F}_1$ is maximized while $\mathcal{F}_2$ is minimized. We treat $\mathcal{F}_1, \mathcal{F}_2$ simultaneous and we put $\mathcal{F}_1$ as the denominator and $\mathcal{F}_2$ as the nominator of a fraction

$$\mathcal{F} = \frac{\mathcal{F}_2}{\mathcal{F}_1}.$$

Fraction $\mathcal{F}$ is now minimized.

Remark 5 In fact, the actual form of $\mathcal{F}$ is slightly different. For term $\mathcal{F}_2$ describing the influence on the neighboring cells one has to take into account four realizations:

- bit 1 is written and is affected by $\mathbf{H}^{90}_{\text{app}}$,
- bit 1 is written and is affected by $\mathbf{H}^{0}_{\text{app}}$,
- bit 0 is written and is affected by $\mathbf{H}^{90}_{\text{app}}$, and
- bit 0 is written and is affected by $\mathbf{H}^{0}_{\text{app}}$.

Thus, in computational implementation, $\mathcal{F}$ takes the form of a sum over all realizations mentioned. For sake of simplicity, we stick to the case when $\mathcal{F}$ is a simple fraction.

Our final aim is to derive Gâteaux derivative of $\mathcal{F}$ with respect to α_L in order to use gradient-type methods for minimization of $\mathcal{F}$. In [19] the authors derived $\frac{\partial \mathcal{F}_i}{\partial \alpha_L}, i = 1, 2$ in terms of solutions ξ_i of two dual problems (denoted by DP_i) defined as linear PDE's with $\mathbf{m}$ as coefficients. Then, one evaluation of $\frac{\partial \mathcal{F}_i}{\partial \alpha_L}$ consists of four steps:

Input: α_L^n

(a) Compute $\mathbf{m}^*$ from the LL equation for α_L^n.
(b) Use $\mathbf{m}^*$ to form two dual problems DP_1 and DP_2.
(c) Compute χ_i as a solution of dual problem DP_i, for $i = 1, 2$.
(d) Compute $\frac{\partial \mathcal{F}_i}{\partial \alpha_L}$ using χ_i. Thus $\frac{\partial \mathcal{F}}{\partial \alpha_L}$ can be evaluated.
(e) Upgrade α_L^n by a suitable algorithm.

Output: α_L^{n+1}

For details see the latter manuscript.

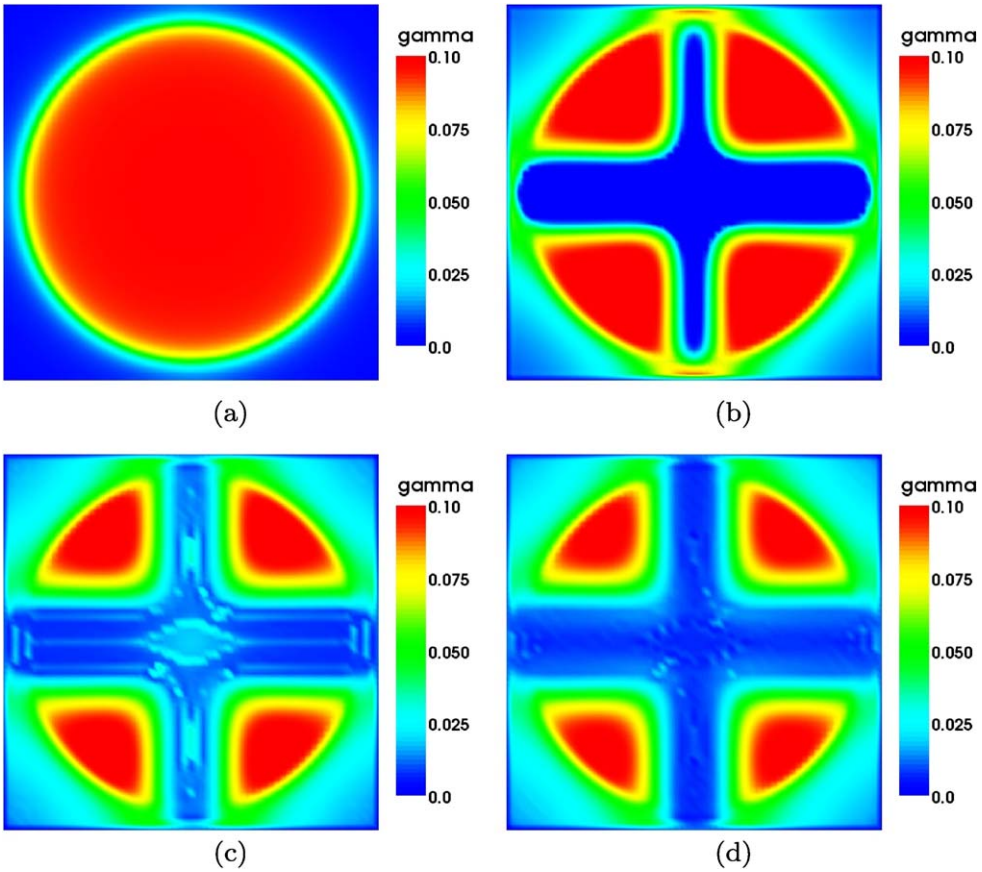

Fig. 5 The evolution of parameter function α_L. (**a**), (**b**), (**c**) and (**d**) depict the initial approximation, the first, the fourth and the sixth iteration, respectively. *Black line* is contour 0.1 which characterizes the boundary of actual shape of the ferromagnetic core. From [19]

Once the explicit form of $\frac{\partial \mathcal{F}}{\partial \alpha_L}$ is known, it is just matter of taste which minimization technique is used for final minimization algorithm. In [19] the steepest descend algorithm was used taking the form

$$\alpha_L^{n+1} = \alpha_L^n - \lambda_n \frac{\partial \mathcal{F}}{\partial \alpha_L}(\alpha_L^n), \tag{19}$$

starting from some initial guess α_L^0 with variable step-size λ_n. The value of λ_n was optimized by a line-search algorithm in every step.

The authors verified the conditions of a general theorem stating the convergence of steepest descend algorithm in real reflexive Banach spaces with $\mathcal{F}$ being Gâteaux-differentiable functional bounded below and increasing, having Lipschitz continuous gradient.

This result guarantees local existence of the minimum only. It would be however too optimistic to find the global minimum, having in mind the complex structure of micromagnetic dynamics.

Actual results of the optimization process are depicted in Fig. 5. The authors used standard $W^{1,2}(\Omega)$-conforming Lagrange finite elements for the approximation of α_L. The final distribution of α_L is such, that mass is greatly reduced along the writing wires where negative effect on the neighboring cells are the most significant, and slightly shifted to the corners of the domain where positive effects of writing by superposed field are dominant.

The representation of γ involving Lagrange finite elements from Fig. 5 does not favor any particular profile of γ. However, in our case we actually seek for a two-valued function γ. Therefore a so called *Level Set Method* can be used for the representation of γ. This method is aimed for the approximation, in general, of a piecewise constant function, in our case of a step function with two values.

For the description of the method see, e.g. [21].

The results from [22] including the Level Set Method are depicted in Fig. 6. They are comparable to the results in Fig. 5, obtained using Lagrange representation of γ. In both cases, the mass is reduced along the writing wires and slightly shifted to the corners of the domain. However, the resulting distributions are different. In the latter case, the interface between the ferromagnetic core and the nonmagnetic background is rendered quite sharply and has different profile.

2 Efficient Numerical Schemes

In the following two sections we provide an overview of known and some new numerical schemes. We focus mainly

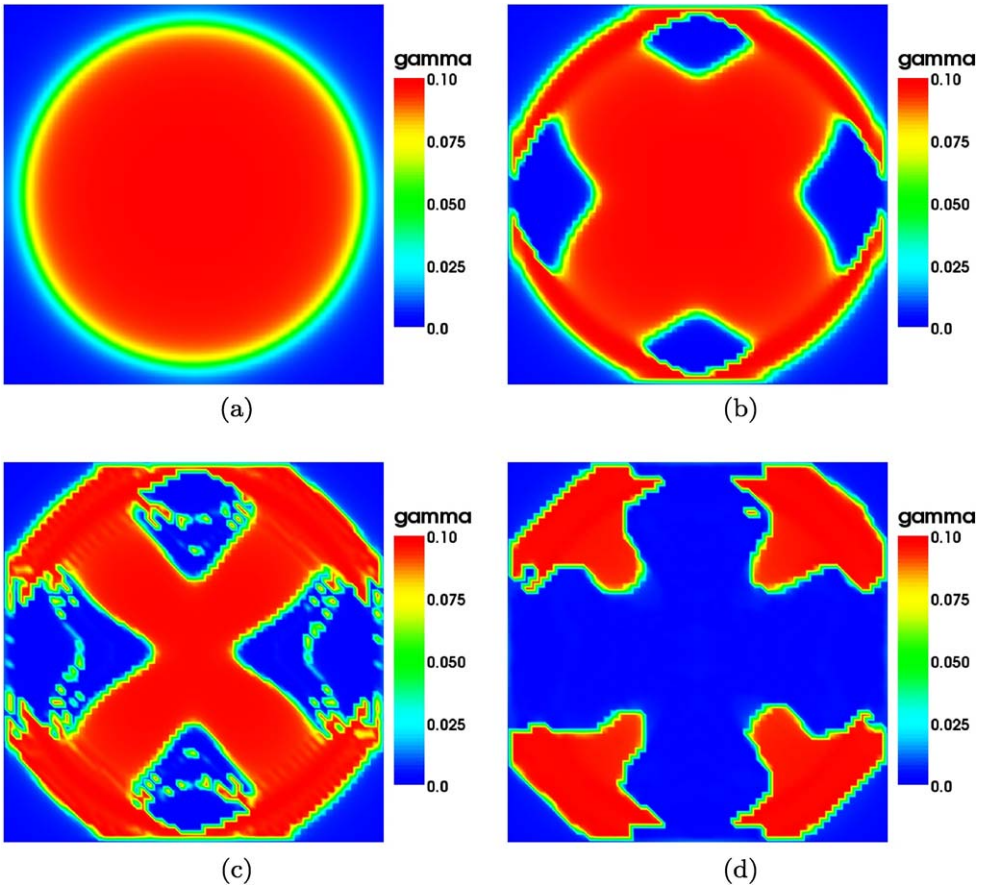

Fig. 6 The parameter function γ; results with LSM representation; (**a**), (**b**), (**c**) and (**d**) depict the initial approximation, the first, the third and the 76th iteration of the steepest descend algorithm, respectively. From [22]

on the case when the exchange field is included in the model and the effective field takes the form $\mathbf{H}_{\text{eff}} = \Delta\mathbf{m}$. If we consider a different scenario we emphasize this explicitly.

From the title of this section one can guess that the efficiency will be main advantage of the schemes discussed in current section. Indeed these schemes have been used already for couple of years giving good results. However, the common disadvantage of these schemes is the lack of reliable convergence results. Schemes, for which convergence results have been obtained, will we addressed in Sect. 3.

The outline of this section is as follows. After couple words about fully implicit backward Euler scheme for the LL equation in Sect. 2.1, we mention a projection scheme of E and Wang. This scheme is quite interesting, because the nonlinear term $|\nabla\mathbf{m}|^2$ is considered as a Lagrange multiplier for the sphere constraint $|\mathbf{m}| = 1$. Therefore, the projection replaces the above mentioned term in the formulation of the LL equation.

Next, in Sect. 2.3, we discuss so called *mid-point rule* based schemes. We show how a general class of magnitude preserving schemes can be derived using Cayley transform and we provide two particular examples of temporal discretizations according to mid-point rule. We call this time discretization a *classical mid-point* and a *classical extrapolated mid-point rule*.

For the beginning let us settle few basic facts. All schemes are based on an equidistant time discretization. This assumption is however not crucial and can be relaxed. Time interval $(0, T_0)$ is split into J time steps of a size $\tau = T_0/J$ and we denote $t_j = j\tau$ for $j = 0, \ldots, J$.

A crucial observation is that $|\mathbf{m}| = 1$ for almost all $t \in \langle 0, \infty)$ provided that the modulus of the initial condition is equal to one too, and that the solution to the LL equation is sufficiently smooth. This comes from a scalar multiplication of the LL equation with $\mathbf{m}$. Then we get $0 = \nabla|\mathbf{m}|^2 = 2\langle\mathbf{m}, \nabla\mathbf{m}\rangle$ and consequently we arrive at

$$0 = \nabla \cdot \langle\mathbf{m}, \nabla\mathbf{m}\rangle = |\nabla\mathbf{m}|^2 + \langle\mathbf{m}, \Delta\mathbf{m}\rangle.$$

Finally, using the previous relation, the term $\mathbf{m} \times (\mathbf{m} \times \Delta\mathbf{m})$, arising in the LL equation when considering the exchange field, according to the vector calculus, can be transformed to

$$\begin{aligned}\mathbf{m} \times (\mathbf{m} \times \Delta\mathbf{m}) &= \langle\mathbf{m}, \Delta\mathbf{m}\rangle\mathbf{m} - |\mathbf{m}|^2\Delta\mathbf{m} \\ &= -|\nabla\mathbf{m}|^2\mathbf{m} - \Delta\mathbf{m}. \end{aligned} \tag{20}$$

This transformation is a classical approach used for example in [6, 23, 24] and gives rise to new ideas when designing numerical schemes.

2.1 Fully Implicit Backward Euler Scheme

Besides standard explicit schemes such as Euler, linear multi-step methods (e.g. Adams-Bashforth, Adams-Moulton, Crank-Nicholson, Backward Differentiation Formulas (BDF)) or Runge-Kutta methods, one can think of a more stable implicit scheme. The first idea that comes on mind is to consider the following fully implicit scheme

$$\delta \mathbf{m}^{j+1} = -\beta_L \mathbf{m}^{j+1} \times \mathbf{H}_{\text{eff}}^{j+1} - \alpha_L \mathbf{m}^{j+1} \times \left(\mathbf{m}^{j+1} \times \mathbf{H}_{\text{eff}}^{j+1} \right). \tag{21}$$

Of course, this scheme suffers from several problems: It does not conserve the magnitude of $\mathbf{m}^j$, its implicit character, after space discretization, implies solving of a nonlinear system, and the last but not least, there has not been proved any convergence results nor error estimates for this scheme.

In fact, this scheme does not belong to this section, since it is not reliable (in the sense that there are no error estimates) and is not even efficient (in the sense that it is necessary to solve a nonlinear system). We added this scheme only for the sake of completeness.

2.2 Projection Based Schemes

A very natural but naive manner how to keep the magnitude of $\mathbf{m}^j$ constant is to renormalize it after each step of time discretization or after a prescribed tolerance has been exceeded, see Fig. 7a. This approach is however a nonlinear numerical modification of the LL time evolution which might have relatively strong effect on the subsequent computation of magnetostatic field [25] and for this reason it is not recommended, especially when long time regimes have to be studied.

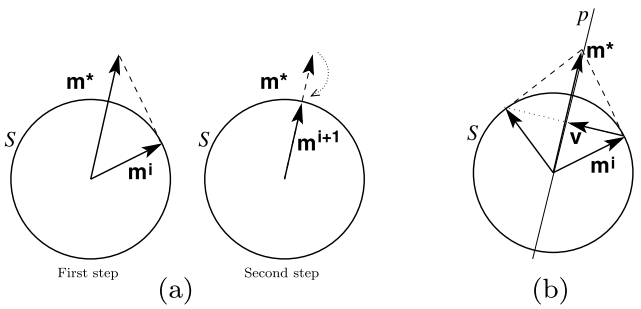

Fig. 7 (**a**) Naive projection schemes use in the first step some numerical scheme giving an intermediate solution $\mathbf{m}^*$ that no longer lives on the unit sphere S. In the second step this intermediate solution is projected back onto sphere S by $\mathbf{m}^{i+1} = \mathbf{m}^* |\mathbf{m}^*|^{-1}$. (**b**) Another approach uses classical backward Euler to get out of the sphere S obtaining vector $\mathbf{m}^*$ with modulus bigger than one. Then using vectorial calculus based on the reflection with respect to axis p one returns $\mathbf{m}^*$ back to the sphere S and thus $\mathbf{m}^{i+1}$ has again modulus one. The problem is that while computing $\mathbf{m}^{i+1}$ one has to gain vector $\mathbf{v}$ which is possible only by a multiplication of $\mathbf{m}^*$ with a coefficient including the length of $\mathbf{m}^*$ in denominator. In this stage, it becomes analogue to the projection scheme

An other idea, trying to avoid the renormalization that keeps the magnitude constant, is explained in Fig. 7b. It uses special symmetry projection to get back on the sphere instead of simply renormalizing of the out-of-the-sphere vector. However, it turns out that in actual computations of the symmetry projection a kind of renormalization has to be used, so this idea does not bring any improvement.

An interesting trick, actually using the renormalization, is suggested by E and Wang [26]. The clever idea is to view the term $|\nabla \mathbf{m}|^2$ in (20) as the Lagrange multiplier for the pointwise constraint $|\mathbf{m}| = 1$. They start from the equation (9) considering $\mathbf{H}_{\text{eff}} = \Delta \mathbf{m}$ with the term $\mathbf{m} \times (\mathbf{m} \times \Delta \mathbf{m})$ transformed according to (20)

$$\mathbf{m}_t + \alpha_C \mathbf{m} \times \mathbf{m}_t = \beta_C (\Delta \mathbf{m} + |\nabla \mathbf{m}|^2 \mathbf{m}).$$

The proposed scheme consists of two steps. First, the term $|\nabla \mathbf{m}|^2$, since it is considered as the Lagrange multiplier, is removed from the equation and a simple linear equation

$$\frac{\mathbf{m}^* - \mathbf{m}^j}{\tau} + \alpha_C \mathbf{m}^j \times \frac{\mathbf{m}^* - \mathbf{m}^j}{\tau} = \beta_C \Delta \mathbf{m}^*$$

accompanied by corresponding BC's is solved to obtain an intermediate magnetization field $\mathbf{m}^*$. The intermediate field $\mathbf{m}^*$ is then projected to the sphere to obtain the numerical solution at the next time step

$$\mathbf{m}^{j+1} = \frac{\mathbf{m}^*}{|\mathbf{m}^*|}.$$

In such a way the projection actually replaces the term $|\nabla \mathbf{m}|^2$ in the original equation.

For the latter scheme E and Wang proved that the scheme is unconditionally stable and convergent in $L^\infty(I, L^\infty(\Omega))$ with first order accuracy. The price the authors have to pay for quite easy proof, was the assumption on existence of the exact solution, with quite high regularity, namely $L^\infty(I, W^{3,2}(\Omega))$.

Further, they present also a modification with second order accuracy which is no more unconditionally stable.

Remark 6 The idea of viewing the term $|\nabla \mathbf{m}|^2$ as a Lagrange multiplier was later discussed also in the framework of weak solutions for the harmonic map heat flow. For more details see Sect. 3.5.2.

2.3 Mid-Point Based Schemes

The LL equation can be rewritten in the following form

$$\mathbf{m}_t = \mathbf{m} \times \mathbf{a}, \tag{22}$$

which is obtained by taking $\mathbf{a} = \beta_L \mathbf{H}_{\text{eff}} + \alpha_L \mathbf{m} \times \mathbf{H}_{\text{eff}}$. In such a form, the evolution on the sphere becomes even more evident. A classical explicit intergator will update $\mathbf{m}$ at time t_j using the approximation

$$\mathbf{m}^{j+1} = \mathbf{m}^j + \mathbf{F}(\mathbf{m}^j, t_j, \tau).$$

The particular form of $\mathbf{F}$ depends on the scheme. However, such an update correspond to translations of $\mathbf{m}^j$, not rotations. Thus a classical explicit integrator does not account for the fact that $\mathbf{m}$ evolves on a sphere.

Another observation is that the component of $\mathbf{a}$ parallel to $\mathbf{m}$ does not influence the solution. However, this component does alter the discrete trajectories generated by numerical algorithms. An appropriate selection of the normal component can improve the performance of the scheme.

An interesting idea is to seek methods that in effect decouple the accuracy of an integrator from the property of conservation of magnitude of magnetization. This approach uses Cayley transform to construct a lifting of the LL equation to a space of fields with values in skew symmetric matrices [25, 27, 28]. A brief sketch of the approach follows.

2.3.1 *Cayley Transform*

Any spatial discretization of (22) leads to the following system of ODE's

$$\dot{\mathbf{M}}_i = \mathbf{M}_i \times \mathbf{A}_i, \tag{23}$$

where $\mathbf{M}_i = \mathbf{M}_i(t)$ and $\mathbf{A}_i = \mathbf{A}_i(t)$ are vectors resulting from the space discretization of $\mathbf{m}$ and $\mathbf{a}$. Consider the standard isomorphism between vectors in $\mathbb{R}^3$ and 3×3 skew symmetric matrices $\text{skew}[\,\cdot\,] : \mathbb{R}^3 \to so(3)$ where $so(3)$ denotes Lie algebra of 3×3 skew symmetric matrices, defined by

$$\mathbf{x} = \begin{pmatrix} x_1 \\ x_2 \\ x_3 \end{pmatrix} \to \text{skew}[\mathbf{x}] = \begin{pmatrix} 0 & -x_3 & x_2 \\ x_3 & 0 & -x_1 \\ -x_2 & x_1 & 0 \end{pmatrix}.$$

Using the elementary identity $\mathbf{x} \times \mathbf{y} = \text{skew}[\mathbf{x}]\mathbf{y}$, we can rewrite (23) as

$$\dot{\mathbf{M}}_i = -\text{skew}[\mathbf{A}_i]\mathbf{M}_i. \tag{24}$$

Knowing that $\mathbf{M}_i(t)$ evolves on the sphere S^2, there is a curve $\Phi_i(t)$ evolving on the Lie group of 3×3 rotation matrices satisfying

$$\mathbf{M}_i(t) = \Phi_i(t)\mathbf{M}_i(0),$$

and $\Phi_i(0) = \mathbb{I}$, the 3×3 identity matrix. We end up with the following system for $\Phi_i(t)$ obtained from (24)

$$\dot{\Phi}_i(t) = -\text{skew}[\mathbf{A}_i]\Phi_i(t). \tag{25}$$

Given any element Φ of $so(3)$ not within the set of measure zero $\{P \in so(3) : -1 \in \textit{spectrum}(P)\}$, one can write

$$\Phi = (\mathbb{I} - 1/2\Psi)^{-1}(\mathbb{I} + 1/2\Psi), \tag{26}$$

where the unique Ψ belongs to $so(3)$.

The actual idea of lifting is very straightforward: derive a differential equation for Ψ_i in (26) where Φ_i satisfies (25).

We remark that the Lie bracket $[\cdot, \cdot]$ is defined as a matrix commutator satisfying

$$\begin{aligned}[\text{skew}[\mathbf{x}], \text{skew}[\mathbf{y}]] &= \text{skew}[\mathbf{x} \times \mathbf{y}] \\ &= \text{skew}[\mathbf{x}]\text{skew}[\mathbf{y}] - \text{skew}[\mathbf{y}]\text{skew}[\mathbf{x}].\end{aligned}$$

Introducing the notation $\text{cay}(\Psi) = (\mathbb{I} - 1/2\Psi)^{-1}(\mathbb{I} + 1/2\Psi)$ we can show

$$\dot{\Psi}_i = -\text{skew}[\mathbf{A}_i] + \frac{1}{2}\big[\Psi_i, \text{skew}[\mathbf{A}_i]\big] + \frac{1}{4}\Psi_i \text{skew}[\mathbf{A}_i]\Psi_i, \tag{27}$$

where

$$\mathbf{M}_i(t) = \text{cay}\Psi_i(t)\mathbf{M}_i(0). \tag{28}$$

Each of the ODE's in (27) evolves in a flat space of 3×3 skew symmetric matrices and we call it the Cayley lift of the space discretized LL dynamics.

The Cayley lift has effectively decoupled the conservation property from the question of accuracy. Indeed, the discrete dynamics (27) can be integrated using methods of required accuracy and unconditional stability will be achieved by suitable implicit schemes (with corresponding computational costs, of course). Simultaneously, the function evaluations (28) automatically conserve magnitude of magnetization.

One possibility to integrate the Cayley lift is to use Cayley transform implicit scheme

$$\begin{aligned}\mathbf{M}_i^{j+1} = &\left(\mathbb{I} + \frac{\tau}{2}\text{skew}[A_i^{j+1/2}]\right)^{-1} \\ &\times \left(\mathbb{I} - \frac{\tau}{2}\text{skew}[A_i^{j+1/2}]\right)\mathbf{M}_i^j,\end{aligned}$$

where the upper index j correspond to temporal discretization with time-step τ.

The previous scheme yields the same numerical scheme as the widely used mid-point rule scheme for (22). We denote the backward Euler approximation of time derivative by $\delta\mathbf{m}$, and the arithmetic mean of two in time consequent approximations steps by $\mathbf{m}^{j+1/2}$, namely take

$$\mathbf{m}_t \approx \delta\mathbf{m}^{j+1} := \frac{\mathbf{m}^{j+1} - \mathbf{m}^j}{\tau}$$

and

$$\mathbf{m}^{j+1/2} := \frac{\mathbf{m}^j + \mathbf{m}^{j+1}}{2}.$$

Using the previous notation, the mid-point scheme reads as

$$\delta\mathbf{M}_i^{j+1} = \mathbf{M}_i^{j+1/2} \times \mathbf{A}_i^{j+1/2},$$

having the property of conserving the modulus of the magnetization. This property can be verified by scalar multiplication of the previous equation with $\mathbf{M}$ which results in

$$\langle \delta\mathbf{M}_i^{j+1}, \mathbf{M}_i^{j+1/2} \rangle = 1/2\tau^{-1}(|\mathbf{M}_i^{j+1}|^2 - |\mathbf{M}_i^j|^2) = 0.$$

Lewis and Nigam [25] study the LL lifting in more general setting. The crucial ingredient in their work is a trivial observation: *The solutions of system* (24) *are not affected by the component of* $\mathbf{A}_i$ *parallel to* $\mathbf{M}_i$. *For numerics, however, it plays a significant role when a correction term parallel to* $\mathbf{M}_i$ *is added to* $\mathbf{A}_i$.

Lewis and Nigam use this observation and instead of considering (24) they depart from the following equation

$$\dot{\mathbf{M}}_i = -\text{skew}[\boldsymbol{\omega}_i]\mathbf{M}_i,$$

where $\boldsymbol{\omega}_i = \mathbf{A}_i + \sigma(\mathbf{M}_i)\mathbf{M}_i$. The freely-to-choose function σ is used for the minimization of the discretization error. In [25] the authors illustrate the influence of the choice for σ on the discrete trajectories determined by the forward Euler algorithm when applied to the LL model. In more detail, where damping plays a crucial role in the long-term dynamics, large values of σ cause the trajectories to sharply diverge from those of the ordinary forward Euler; however, the final state is the same. A closer look at the LL equation shows that a larger value of σ corresponds to the inclusion of more precession in the trajectory. These statements are verified by numerical results presented in [25]. The authors present also a general geometric approach for selecting values for σ and show that when used with the forward Euler method, this choice of σ minimizes the discretization error.

2.3.2 Mid-Point Rule

The methods based on the Cayley lift preserve the magnetization amplitude, but they do not generally preserve other important physical features of the LL equation mentioned in Sect. 1.3 such as the Liapounov and the Hamiltonian structure. Therefore we will focus on one particular scheme called *mid-point rule* which does preserve the Liapounov and the Hamiltonian structure. When considering only temporal discretization, the mid-point rule scheme reads as

$$\delta\mathbf{m}^{j+1} = \mathbf{m}^{j+1/2} \times \mathbf{a}^{j+1/2}. \tag{29}$$

Monk and Vacus [29] use the mid-point rule scheme for the LL part of the coupled Maxwell-Landau-Lifshitz system mentioned in Sect. 1.4.1. However, they study a simplified case when only anisotropy field is included in the LL model. Then, the LL equation becomes an ordinary differential equation. The authors show that their scheme conserves the magnitude of $\mathbf{m}$ and verify the Liapounov structure of the scheme.

In Table 1 with comparison of several schemes we refer this scheme as classical mid-point rule.

In their later work [9] they go further and add the exchange field into consideration. However, for fully discrete scheme involving the temporal discretization they do not show any convergence results nor they prove error estimates.

A wide numerical study of the mid-point rule scheme (29) is performed by d'Aquino, Serpico and Miano [5]. They consider full version of the effective field, i.e., anisotropy, exchange, applied and demagnetizing fields are involved in the LL model. Especially the last one, due to its nonlocal character, can cause problems in actual computations.

Remark 7 This work, however, considers strong solutions of the LL equation. That means that when the exchange field is involved, the solution $\mathbf{m}$ must exist in $W^{2,2}(\Omega)$ space. This is not always the case, e.g. for less regular initial data. In that case, one has to switch to weak formalism and use the schemes of Prohl and Bartels, see Sects. 3.3–3.7.

The authors suggest space discretization by finite differences or finite elements and show that fully discretized scheme conserves the magnitude of $\mathbf{m}$, preserves the Liapounov structure of the LL system, and in case of $\alpha_G = 0$ preserves the Hamiltonian structure.

The above mentioned properties are strongly related to the implicit nature of fully discretized mid-point rule scheme. This implicit nature results in the necessity of solving a nonlinear system of equations on each time step.

d'Aquino et al. circumvent this problem by using special and reasonably fast quasi-Newton iterative technique.

The slightly modified version of mid-point rule scheme is used also by Serpico, Mayergoyz and Bertotti [30]. Instead of taking $\mathbf{a}^{j+1/2}$ they extrapolate the value in time $t_j + \tau/2$ by the formula $3/2\mathbf{a}^j - 1/2\mathbf{a}^{j-1}$ which is accurate up to the second order. They eventually obtain a numerical scheme with the truncation error of second order of smallness with respect to τ,

$$\delta\mathbf{m}^{j+1} = \mathbf{m}^{j+1/2} \times \left(\frac{3}{2}\mathbf{a}^j - \frac{1}{2}\mathbf{a}^{j-1}\right). \tag{30}$$

In Table 1 with comparison of several schemes, we refer this scheme as classical extrapolated mid-point rule.

Table 1 Overview of the properties of particular numerical schemes. The second column informs about the conservation of $|\mathbf{m}^i|$ on each time step. Term *asympt.* means that the modulus is asymptotically conserved in some norm when time-step τ tends to zero. Information about the convergence analysis of the scheme is provided in the third column. Term *asympt. anal.* stands for the asymptotic analysis mentioned in Remark 4. Term *converg.* means that there were derived convergence results to the solution, whereas *error est.* means that error estimates are available. In the fourth column we mention if corresponding convergence analysis was done assuming existence and regularity of strong solutions or only weak solutions. In the last column we inform in which section the particular scheme was mentioned

Type of the scheme	$\lvert\mathbf{m}^i\rvert = const$	Convergence analysis	Week/strong solutions	Section
Fully implicit backward Euler scheme (21)	No	Asympt. anal.	Strong	2.1
Projection scheme of E and Wang	Yes	Asympt. anal.	Strong	2.2
Classical mid-point rule (29)	Yes	Asympt. anal.	Strong	2.3.2
Extrapolated classical mid-point rule (30)	Yes	Asympt. anal.	Strong	2.3.2
Semi-implicit with penalization terms (31)	Asympt.	Error est.	Strong	3.1
Semi-implicit with exact formula on one time level	Asympt.	Error est.	Strong	3.1
Alouges-Jaisson Algorithm 1	Yes	Converg.	Weak	3.3
Bartels-Prohl Algorithm 3	Yes	Converg.	Weak	3.4
Bartels-Prohl Algorithm 8 for LL form	Yes	Converg.	Weak	3.6

3 Reliable Numerical Schemes

After the presentation of methods suffering from the lack of reliability in Sect. 2, we go on and we review schemes for which convergence results or error estimates has been obtained. The schemes described in this section can be divided into two groups. In the first group, we have two schemes: Semi-implicit scheme (31) and semi-implicit scheme with exact formula for the solution on one time level from Sect. 3.1. Both schemes require the existence of strong solutions with some regularity. Schemes in the second group deal with weak solution and therefore are of more practical use. The second group consists of Alouges-Jaisson Algorithm 1 from Sect. 3.3, of Bartels-Prohl Algorithm 3 from Sect. 3.4 and modified Bartels-Prohl Algorithm 8 from Sect. 3.6.

We will focus on the latter group since the methods guaranteeing convergence to weak solutions are much more practical than those dealing with strong solutions. Usually it is mathematically more difficult—and therefore also more interesting—to deal with weak solutions since they have less regularity than strong solutions. A significant step forward in the convergence theory of mid-point based schemes has been done only recently in 2006 by Alouges and Jaisson and a short time later by Prohl and Bartels. The latter couple propose fully discrete schemes, using reduced integration, for which they showed convergence to the weak solutions in corresponding functional spaces. We discuss these methods in more detail in Sects. 3.3–3.7.

The outline of this section is as follows. First, in Sect. 3.1 we describe semi-implicit methods dealing with strong solutions. In the next subsection we provide the definition of weak solutions to the LL equation together with some notations. We introduce reduced integration and we list several interpolation estimates for reduced integration. Further we define a discrete Laplace operator acting on less regular functions from $W^{1,2}(\Omega)$ and we also provide some basic properties of this operator.

In Sect. 3.3 we discuss the first numerical scheme dealing with weak solutions for which convergence results have been obtained. However, the convergence was obtained for two limit processes one after the other: First for time-step τ going to zero and then for mesh size h going to zero.

Further in Sect. 3.4 we examine the cross-product type schemes introduced by Bartels and Prohl. For this schemes, limit was obtained simultaneously for $(\tau, h) \to 0$. This scheme is however nonlinear and thus subsequent linearization is provided.

In Sect. 3.5 we discuss slightly different topic of harmonic map heat flow, however it turns out that the ideas from this area can be repeated in the LL setting, see Sect. 3.6.

Finally, we provide recent results on the full Maxwell-LL system. The coupling of Maxwell equations with the LL equation is a nontrivial task and we present a successful attempt to design a numerical scheme dealing with weak solutions to the Maxwell-LL system in Sect. 3.7.

3.1 Semi-Implicit Schemes

The transformation leading to (20) suggests the time discretization

$$\delta \mathbf{m}^{j+1} - \alpha_L \Delta \mathbf{m}^{j+1} = -\beta_L \mathbf{m}^j \times \Delta \mathbf{m}^{j+1} + \alpha_L |\nabla \mathbf{m}^j|^2 \mathbf{m}^{j+1}. \tag{31}$$

We can directly observe that the scheme is linear so no implementation of a nonlinear solver is needed. Further, in [6] for 2D and in [7] for 3D, the authors have obtained the error estimates in the case of the existence of strong solutions for the single LL equation. They also state the conditions when strong solutions exist. The order of convergence obtained is $o(\tau)$ for the $L^\infty(I, L^2(\Omega))$ norm and is $o(\tau^{1/2})$ for the $L^2(I, W^{1,2}(\Omega))$ norm. The case of coupled Maxwell-LL system was discussed in [31–33].

However, this scheme fails to conserve the modulus of $\mathbf{m}^j$. Indeed, the only information about the length of $\mathbf{m}^j$ is asymptotic, namely the difference

$$\max_{0\le j\le J} \|1 - |\mathbf{m}^j|^2\|_2$$

is of order $o(\tau)$.

The strategy to obtain better error estimates is to introduce penalization terms. The idea of penalization in order to satisfy some constraint is not new and has appeared in many areas. Prohl [6] has added a penalization term $\Phi(\mathbf{m}^i, \mathbf{m}^{i+1})$ to the scheme (31) arriving at

$$\delta \mathbf{m}^{j+1} - \alpha_L \Delta \mathbf{m}^{j+1} + \frac{1}{\varepsilon}\Phi(\mathbf{m}^i, \mathbf{m}^{i+1}) = -\beta_L \mathbf{m}^j \times \Delta \mathbf{m}^{j+1} + \alpha_L |\nabla \mathbf{m}^j|^2 \mathbf{m}^{j+1}.$$

In the overview Table 1 we call this scheme as semi-implicit scheme with penalization terms.

To satisfy the constraint $|\mathbf{m}^j| = 1$ there exist more choices for Φ,

$$\Phi_1(\mathbf{m}^i, \mathbf{m}^{i+1}) = |\mathbf{m}^{j+1}|^2 - 1,$$
$$\Phi_2(\mathbf{m}^i, \mathbf{m}^{i+1}) = 1 - |\mathbf{m}^{j+1}|^{-2},$$
$$\Phi_3(\mathbf{m}^i, \mathbf{m}^{i+1}) = 1 - |\mathbf{m}^{j+1}|^{-1}.$$

The first choice called *Ginzburg-Landau approximation* was already helpful for the proof of existence of weak solutions to LL equation in 3D [34, 35]. For all three choices Φ_1, Φ_2, Φ_3 Prohl has proved in 2D setting the convergence rate $o(\tau^{1/2}\varepsilon^{1/4})$ in $L^4(I, L^4(\Omega))$ together with estimate for the asymptotic conservation of the modulus guaranteeing that

$$\max_{0\le j\le J} \|1 - |\mathbf{m}^j|^2\|_2$$

is of order $o(\tau^{1/2}\varepsilon^{1/2})$.

The differences between particular choices of Φ were only in the dependence of ε on τ. For Φ_1 it is necessary that $\varepsilon^{-1} = o(\tau^{-1})$, for Φ_2 was the estimate sharpened to $\varepsilon > 1.9\tau$ and finally for Φ_3 it is $\varepsilon \ge \tau$.

It would be somehow straightforward to extend the results to 3D setting.

An interesting approach in numerics leaves from the special structure of the LL equation (22). The following lemma [36] gives the explicit solution of (22) when $\mathbf{a}$ is known.

Lemma 1 *Let* $\mathbf{a}$ *and* $\mathbf{u}_0$ *be any vectors in* $\mathbb{R}^3$. *Then the unique solution of* $\mathbf{m}_t = \mathbf{m} \times \mathbf{a}$, $t > 0$, *for* $\mathbf{u}(0) = \mathbf{u}_0$, *is given by*

$$\mathbf{m}(t) = \exp(at) \times \mathbf{m}_0 = \mathbf{m}_0^{\parallel} + \mathbf{m}_0^{\perp} \cos(|\mathbf{a}|t) + \sin\frac{\mathbf{a}}{|\mathbf{a}|} \times \mathbf{m}_0^{\perp} \sin(|\mathbf{a}|t)$$

for $\mathbf{m}_0 = \mathbf{m}_0^{\perp} + \mathbf{m}_0^{\parallel}$ *where* $\mathbf{m}_0^{\parallel}$ *is parallel to* $\mathbf{a}$ *and* $\mathbf{m}_0^{\perp}$ *is perpendicular to* $\mathbf{a}$.

The previous lemma suggests to use an alternative way of the time discretization. Namely, one does not have to approximate the time derivative in the LL equation by backward Euler approximation. Instead, we reformulate the LL equation into the form $\mathbf{m}_t = \mathbf{m} \times \mathbf{a}$, with the initial condition $\mathbf{m}(0) = \mathbf{m}^j$ and for the computation of $\mathbf{m}^{j+1}$ we use Lemma 1 which provides the exact formula for the solution on one time level. For the evaluation of $\mathbf{a}$ we use the values obtained from the previous time step putting $\mathbf{a} = \beta_L \mathbf{H}_{\text{eff}}(t_j) + \alpha_L \mathbf{m}(t_j) \times \mathbf{H}_{\text{eff}}(t_j)$.

Disadvantage of this scheme is that it is an explicit scheme. So it would be difficult to obtain any error estimates for the case when the exchange field is included in the model.

For the case of single Landau-Lifshitz equation without the exchange field, in [37] the authors derive the error estimates in $L^\infty(I, L^2(\Omega))$ obtaining rate of convergence $o(\tau^2)$.

For the case of the coupled Maxwell-Landau-Lifshitz system the exchange field, a numerical study was performed [36, 38–40]. The authors implemented the above mentioned idea and showed the error estimates in $L^\infty(I, L^2(\Omega))$ and in $L^2(I, H(\mathbf{curl}, \Omega))$ for the magnetic field and in $L^\infty(I, L^2(\Omega))$ for the magnetization. The rate of the convergence was $o(\tau^{1/2})$ for the full Maxwell system and $o(\tau)$ for the quasi-static case of Maxwell equations.

In the overview Table 1 we refer this scheme as semi-implicit scheme with exact formula on one time step.

3.2 Weak Solutions to the LL Equation and Some Preliminaries

Since in this section we address the convergence of numerical schemes to the weak solution of the LL equation, we recall the definition taken from [34].

Definition 1 Given $\mathbf{m}_0 \in W^{1,2}(\Omega)$ such that $|\mathbf{m}_0| = 1$ almost everywhere in Ω, a function $\mathbf{m}$ is called *a weak solution of (8)* if for all positive T there holds (i) $\mathbf{m} \in H^1(\Omega_T, \mathbb{R}^3)$ with $\mathbf{m}(0,\cdot) = \mathbf{m}_0$ in the sense of traces, (ii) $|\mathbf{m}| = 1$ almost everywhere in Ω_T, (iii) for almost all $T' \in (0, T)$ there holds

$$\frac{1}{2}\int_\Omega |\nabla \mathbf{m}(T', x)|^2 \mathrm{d}x + \frac{\alpha_L}{\alpha_L^2 + \beta_L^2}\int_0^{T'} \|\mathbf{m}_t\|_2^2 \mathrm{d}t \leq \frac{1}{2}\int_\Omega |\nabla \mathbf{m}_0(x)|^2 \mathrm{d}x, \tag{32}$$

and, (iv) for all $\phi \in C^\infty(\overline{\Omega}_T, \mathbb{R}^3)$ there holds

$$\int_0^T (\mathbf{m}_t, \phi)\mathrm{d}t - \alpha_G \int_0^T (\mathbf{m} \times \mathbf{m}_t, \phi)\mathrm{d}t = \beta_G \int_0^T (\mathbf{m} \times \nabla \mathbf{m}, \nabla \phi)\mathrm{d}t. \tag{33}$$

Further, all schemes discussed in this section use finite element approach. For clarity we briefly outline the basic notations and preliminaries.

We assume that $\mathcal{T}_h$ is a quasi-uniform regular triangulation of the polygonal or polyhedral bounded Lipschitz domain $\Omega \in \mathbb{R}^n$ into triangles or tetrahedrons for $n = 2$ or $n = 3$, respectively. The diameter of $\mathcal{T}_h$ is denoted by $h = \min\{\mathrm{diam}(K) : K \in \mathcal{T}_h\}$. We define the lowest order finite element space $V_h \subset W^{1,2}(\Omega)$ containing continuous functions that elementwise are polynomials of total degree less or equal to one. We denote $\mathcal{N}_h$ the set of all nodes z of the triangulation $\mathcal{T}_h$ and we introduce the nodal interpolation operator $\mathcal{I}_h : C(\overline{\Omega}, \mathbb{R}^3) \to V_h$ satisfying $\mathcal{I}_h\phi(z) = \phi(z)$ for all $z \in \mathcal{N}_h$. By $\langle\cdot,\cdot\rangle$ we denote the inner product of two vectors in $\mathbb{R}^m$ and we let $(\cdot,\cdot)$ denote the L^2 scalar product of two vector functions. By $\|\cdot\|_p$ we understand the L^p norm for $1 < p \leq \infty$.

The main tool enabling the convergence analysis of midpoint rule methods is so called *reduced integration*. For continuous functions $\theta, \phi \in C(\overline{\Omega}, \mathbb{R}^3)$ we define

$$(\theta, \phi)_h = \int_\Omega \mathcal{I}_h(\langle\theta, \phi\rangle)\mathrm{d}x = \sum_{z\in\mathcal{N}_h} \beta_z \langle\theta(z), \phi(z)\rangle, \tag{34}$$

for certain weights β_z. More specific, if for each $z \in \mathcal{N}_h$ we denote by $\varphi_z \in C(\overline{\Omega})$ the nodal basis function which is $\mathcal{T}_h$-elementwise affine and satisfies $\varphi_z(y) = \delta_{zy}$ for all $y \in \mathcal{N}_h$, then we have $\beta_z = \int_\Omega \varphi_z \mathrm{d}x$. We define $\|\phi\|_h^2 = (\phi, \phi)_h$.

Basic interpolation estimates yield

$$\big|(\phi_h, \psi_h)_h - (\phi_h, \psi_h)\big| \leq Ch\|\phi_h\|_2\|\nabla\psi_h\|_2, \tag{35}$$

for all $\phi_h, \psi_h \in V_h$, where $C > 0$ denotes an (h, τ)-independent constant.

Further, we define a discrete Laplace operator $\tilde{\Delta}_h : W^{1,2}(\Omega) \to V_h$ by

$$-(\tilde{\Delta}_h\phi, \chi_h)_h = (\nabla\phi, \nabla\chi_h) \quad \text{for all } \chi_h \in V_h.$$

We list some properties of operator $\tilde{\Delta}_h$ taken from [11]. Denote h the maximal mesh-size of $\mathcal{T}_h$ defined as a maximal diameter of all elements in $\mathcal{T}_h$. It holds

$$\|\nabla\phi_h\|_2 \leq c_1 h^{-1}\|\phi_h\|_2, \tag{36}$$

$$\|\tilde{\Delta}_h\phi_h\|_h \leq c_1 h^{-1}\|\nabla\phi_h\|_2, \tag{37}$$

$$|\tilde{\Delta}_h\phi_h(z)| \leq c_2 h^{-2}\|\phi_h\|_\infty, \tag{38}$$

for some positive c_1, c_2. Piecewise constant interpolations of u^i are defined for $0 \leq t \leq J\tau$ such that if $t \in [i\tau, (i+1)\tau)$ for some i then $\overline{u}(t) := u^{i+1/2}$ and $u^+(t) := u^{i+1}$. Piecewise linear approximation reads as

$$\hat{u}(t) := \frac{t - i\tau}{\tau}u^{i+1} + \frac{(i+1)\tau - t}{\tau}u^i.$$

3.3 Alouges-Jaisson Scheme

First numerical scheme dealing with weak solutions to the LL equation was proposed by Alouges and Jaisson [41]. Beside the notations introduced in Sect. 3.2 we denote $\mathcal{M}_h$ the subset of V_h containing those vector fields that have modulus one in all vertexes of the mesh. Further, for a given discrete magnetization $\mathbf{m}^j$ we introduce the tangent space

$$\mathcal{F}_j = \{\mathbf{w} \in V_h | \langle\mathbf{w}(z), \mathbf{m}^j(z)\rangle = 0, \text{for all } z \in \mathcal{N}_h\}.$$

First step in the construction of the AJ scheme is to rewrite (33) in the definition of weak solution. Taking $\phi = \mathbf{m} \times \mathbf{w}$ in (33) where $\mathbf{w} \in W^{1,2}(\Omega_T)^3 \cap L^\infty(\Omega_t)^3$ satisfies $\langle\mathbf{w}, \mathbf{m}\rangle = 0$ a.e., we get

$$\alpha_G \int_0^T (\mathbf{m}_t, \mathbf{w})\mathrm{d}t + \int_0^T (\mathbf{m} \times \mathbf{m}_t, \mathbf{w})\mathrm{d}t = -\beta_G \int_0^T (\nabla\mathbf{m}, \nabla\mathbf{w})\mathrm{d}t. \tag{39}$$

The original weak formulation can be re-obtained by taking $\mathbf{w} = \mathbf{m} \times \phi$ for any $\phi \in C_0^\infty(\Omega_T)$.

A straightforward discretization of (39) leads to the following problem: $\mathbf{m}^j$ being given, find $\mathbf{m}^{j+1} \in \mathcal{M}_h$ solution

to

$$\alpha_G \int_0^T (\delta \mathbf{m}^{j+1}, \mathbf{w})\mathrm{d}t + \int_0^T (\mathbf{m}^j \times \delta \mathbf{m}^{j+1}, \mathbf{w})\mathrm{d}t$$
$$= -\beta_G \int_0^T (\nabla \mathbf{m}^{j+1/2}, \nabla \mathbf{w})\mathrm{d}t, \quad \text{for all } \mathbf{w} \in \mathcal{F}_j. \tag{40}$$

Due to the constraint on $\mathbf{m}^{j+1}$ it is an uneasy task to solve the latter equation. Alouges and Jaisson suggest the following: On account of the constraint on $\mathbf{m}^{j+1}$, the quantity $\delta \mathbf{m}^{j+1}$ almost belongs to $\mathcal{F}_j$. By replacing $\delta \mathbf{m}^{j+1}$ by an unknown $\mathbf{s}$ which belongs to $\mathcal{F}_j$ we will approximate (40) by

$$\alpha_G \int_0^T (\mathbf{s}, \mathbf{w})\mathrm{d}t + \int_0^T (\mathbf{m}^j \times \mathbf{s}, \mathbf{w})\mathrm{d}t$$
$$= -\beta_G \int_0^T (\nabla \mathbf{m}^j, \nabla \mathbf{w})\mathrm{d}t, \quad \text{for all } \mathbf{w} \in \mathcal{F}_j. \tag{41}$$

The algorithm for the AJ scheme proposed by Alouges and Jaisson consists of two steps:

Algorithm 1

1. $\mathbf{m}^j$ *being given, solve* (41) *obtaining* $\mathbf{s}^j$ *as a solution.*
2. *Compute* $\mathbf{m}^{j+1}$ *from*

$$\mathbf{m}^{j+1} = \frac{\mathbf{m}^j + \tau \mathbf{s}^j}{|\mathbf{m}^j + \tau \mathbf{s}^j|}.$$

The main contribution of this scheme is that although a renormalization takes place in the algorithm, still it is possible to obtain the convergence to the weak solutions.

Note that (41) is only a kind of perturbation of (40). Thus the first step of the AJ algorithm will not actually solve (40). But since in the second step of the algorithm we compute $\mathbf{m}^{j+1}$ by re-normalizing, we actual get closer to the solution of (40). After all, it can be shown by examining the residual $\mathbf{r} = \mathbf{m}^{j+1} - \mathbf{m}^j - \tau \mathbf{v}^j$, that first passing to the limit $\tau \to 0$, and second passing to the limit $h \to 0$ will lead to the convergence (up to subsequence) to the weak solution of the LL equation. Namely, Alouges and Jaisson obtained weak convergence in $W^{1,2}(\Omega_T)$ and strong convergence in $L^2(\Omega_T)$.

Remark 8 The AJ scheme is a first successful attempt to design a scheme actually constructing the weak solutions to the LL equation. The way how the convergence was proved, however, is not of the full practical use. Showing the convergence by examining two limit processes one after the other gives a weaker tool for practical implementations than considering τ and h going to zero simultaneously. Bartels, Ko and Prohl in [42] do prove the convergence of the AJ scheme by passing to the double limit $(\tau, h) \to 0$. Due to the explicit character of the AJ scheme, τ and h are not allowed to go to zero freely. An extra condition

$$\tau h^{-1-n/2} \to 0$$

has to be put in order to show the convergence. In case of three dimensions the condition becomes $\tau h^{-5/2} \to 0$, which is quite restrictive for the computations.

Remark 9 The idea of the AJ scheme can be used for different topics too. Namely, the authors of [43] adapted the AJ scheme for the p-harmonic flow into spheres, see also Sect. 3.5.

3.4 Cross-Product Type Schemes—LLG Form

For the Alouges-Jaisson scheme described in Sect. 3.3, the bound $\tau = o(h^{1+n/2})$ is identified to be sufficient for stability and convergence; sharpness of these restrictions is evidenced by computational studies in [42]. From this background, Bartels and Prohl look for an implicit scheme exempt from restricting requirements for numerical parameters, and with higher flexibility with respect to (small) choices of $\alpha_L > 0$. The construction of a discretization studied in [11] is a mid-point rule based scheme departing from the LLG form (8). They propose the following algorithm.

Algorithm 2 *Given* $\mathbf{m}^j \in V_h$, *find* $\mathbf{m}^{j+1} \in V_h$ *such that for all* $\phi_h \in V_h$ *there holds*

$$(\delta \mathbf{m}^{i+1}, \phi_h)_h - \alpha_G (\mathbf{m}^j \times \delta \mathbf{m}^{i+1}, \phi_h)_h$$
$$= -\beta_G (\mathbf{m}^{i+1/2} \times \tilde{\Delta}_h \mathbf{m}^{i+1/2}, \phi_h)_h. \tag{42}$$

We call this scheme the Bartels-Prohl scheme, see Table 1 for comparison with other schemes.

Remark 10 The linear second term in (42) is motivated by the identity

$$\frac{1}{\tau}\mathbf{m}^j \times \mathbf{m}^{j+1} = \mathbf{m}^j \times \delta \mathbf{m}^{j+1}$$
$$= \left(\mathbf{m}^{j+1/2} - \frac{\tau}{2}\delta \mathbf{m}^{j+1}\right) \times \delta \mathbf{m}^{j+1}$$
$$= \mathbf{m}^{j+1/2} \times \delta \mathbf{m}^{j+1}.$$

From [11] we have the following convergence result.

Theorem 1 *Let* τ *be a positive number, and* $(\mathcal{T}_h)_{h>0}$ *be a family of regular triangulations of* Ω *with maximal mesh-size* h. *Suppose that* (i) $|\mathbf{m}^0(z)| = 1$ *for all nodes* $z \in \mathcal{N}_h$,

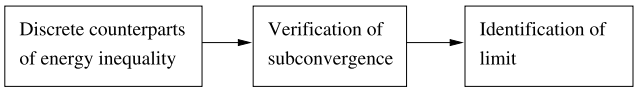

Fig. 8 A typical proof of convergence result consists of three steps: First, the discrete counterparts of the energy inequality from the definition of weak solutions are derived and proved. Second, convergence of a subsequence of the linear interpolants is verified, with some limit function. Third, the limit function is identified to be the weak solution of the particular problem

(ii) *for all* $0 \le i \le J-1$ *and for all* $\phi \in V_h$ *the relation* (42) *holds.*

Then the modulus of $\mathbf{m}^i$ *is preserved, that is,*

$$|\mathbf{m}^j(z)| = 1$$

for all nodes $z \in \mathcal{N}_h$ *and for* $0 \le i \le J$. *If* $J\tau > T$ *and* $\mathbf{m}^0 \to \mathbf{m}_0$ *in* $W^{1,2}(\Omega)$ *for* $h \to 0$ *then, taking* $\hat{\mathbf{m}}_{h,\tau}$ *as a piecewise linear approximation of* $\mathbf{m}^i$, *there exists a subsequence of* $(\hat{\mathbf{m}}_{h,\tau})$ *as* $(h,\tau) \to 0$ *which converges weakly in* $W^{1,2}(\Omega_T)$ *to a weak solution of the LL equation.*

The proof of the convergence relies on three ingredients, see Fig. 8. First, the discrete counterparts of (iii) and (iv) from Definition 1 are proved for the approximate solutions $\mathbf{m}^j$, so that

$$|\mathbf{m}^{j+1}(z)| = 1 \quad \text{for all } z \in \mathcal{N}_h, \tag{43}$$

$$\frac{1}{2}\delta\|\nabla\mathbf{m}^{j+1}\|_2^2 + \frac{\alpha_L}{\alpha_L^2+\beta_L^2}\|\delta\mathbf{m}^{j+1}\|_2^2 = 0. \tag{44}$$

Then, using the notations from Sect. 3.2, the following types of convergence to some $\mathbf{m}$ can be proved, up to the subsequence

$$\begin{aligned}
&\hat{\mathbf{m}} \rightharpoonup \mathbf{m} \quad \text{in } W^{1,2}(\Omega_T),\\
&\overline{\mathbf{m}} \to \mathbf{m} \quad \text{in } L^2(\Omega_T),\\
&\nabla\overline{\mathbf{m}} \rightharpoonup \nabla\mathbf{m} \quad \text{in } L^2(\Omega_T),\\
&\mathbf{m}^+ \rightharpoonup^* \mathbf{m} \quad \text{in } L^\infty((0,T), W^{1,2}(\Omega)).
\end{aligned} \tag{45}$$

Third, one has to identify the limit $\mathbf{m}$. Departing from (42) it is possible to show by combining of the properties of $(\cdot,\cdot)_h$, $W^{1,2}(\Omega)$-stability of $\mathcal{I}_h$, convergence results (45), and interpolation estimates (36)–(38) that $\mathbf{m}$, as a limit of $\{\hat{\mathbf{m}}_{h,\tau}\}$, is a weak solution to the LL equation.

Algorithm 2 however involves solving of a nonlinear system. In [11] the authors suggest the following fixed-point iteration to solve the nonlinear system

Algorithm 3 *Given* $\mathbf{m}^j \in V_h$, *set* $\mathbf{m}^{j+1,0} = \mathbf{m}^j$ *and* $l = 0$.

(a) *Compute* $\mathbf{m}^{j+1,l+1} \in V_h$, *such that for all* $\phi \in V_h$ *there holds*

$$\begin{aligned}
&\frac{1}{\tau}(\mathbf{m}^{j+1,l+1},\phi)_h + \frac{\alpha_G}{\tau}(\mathbf{m}^j \times \mathbf{m}^{j+1,l+1},\phi)_h\\
&\quad + \frac{\beta_G}{4}(\mathbf{m}^{j+1,l+1} \times \tilde{\Delta}_h\mathbf{m}^{j+1,l},\phi)_h\\
&\quad + \frac{\beta_G}{4}(\mathbf{m}^{j+1,l+1} \times \tilde{\Delta}_h\mathbf{m}^{j},\phi)_h\\
&\quad + \frac{\beta_G}{4}(\mathbf{m}^{j} \times \tilde{\Delta}_h\mathbf{m}^{j+1,l+1},\phi)_h\\
&= -\frac{\beta_G}{4}(\mathbf{m}^j \times \tilde{\Delta}_h\mathbf{m}^j,\phi)_h + \frac{1}{\tau}(\mathbf{m}^j,\phi)_h.
\end{aligned}$$

(b) *If* $\|\mathbf{m}^{j+1,l+1} - \mathbf{m}^{j+1,l}\|_h \le \varepsilon$, *then stop and set* $\mathbf{m}^{j+1} = \mathbf{m}^{j+1,l+1}$.

(c) *Set* $l := l+1$ *and go to* (a).

Using an $(h,\tau,\alpha_G,\beta_G)$-independent constant c depending only on the geometry of $\mathcal{T}_h$ one can show the following property

$$\|\mathbf{m}^{j+1,l+1} - \mathbf{m}^{j+1,l}\|_h \le \frac{1}{c}\tau h^{-2}\beta_G\|\mathbf{m}^{j+1,l} - \mathbf{m}^{j+1,l-1}\|_h.$$

If we require that $\tau \le ch^2/\beta_G$ then, according to the previous inequality, the sequence $\{\mathbf{m}^{j+1,l}\}_{l=1}^\infty$ becomes contractive and consequently we can apply the Banach fixed-point theorem. This means that if $|\mathbf{m}^j(z)| = 1$ for all $z \in \mathcal{N}_h$, than a unique $\mathbf{m}^{j+1,*} \in V_h$ exists, which solves also Algorithm 2.

Remark 11 The obvious disadvantage is that in the computations, when applying the fixed-point technique from Algorithm 3, we get only an approximation of the unique $\mathbf{m}^{j+1,*}$, so Algorithm 2 is not satisfied exactly. For practical computations, however, at most five iterations were needed to reach quite sharp stopping criterion $\varepsilon = h^4$. The computations [11] were performed on an example with discontinuity in $W^{1,2}(\Omega)$ norm, which was designed for a numerical tracement of the blow-up.

The above mentioned disadvantage has been overcome by Bartels [44]. He uses the idea from Algorithm 5 of introducing a small perturbation with an appropriate vector product structure, see Sect. 3.5.

An alternative approach to the LL equation departs from the approximation of the LL form instead of the LLG form. We describe this approach later in Sect. 3.6 since it uses the idea appearing in the work [45]. Therefore we jump into the topic of the harmonic map heat flow into spheres to introduce the above mentioned idea. Then, we will come back and we provide Algorithm 7 with the corresponding fixed-point Algorithm 8, which is designed in such a way, that fixed-point iterations actually preserve the magnitude of $\mathbf{m}^{j,l}$.

3.5 Harmonic Map Heat (HMH) Flow into Spheres

The structure of the LL equation has an interesting property: For the effective field, consider the exchange field only, so $\mathbf{H}_{\text{eff}} = \Delta\mathbf{m}$. Then, when taking the limit $\beta_L \to 0$ one gets the following equation

$$\mathbf{m}_t = -\alpha_L \mathbf{m} \times (\mathbf{m} \times \Delta\mathbf{m}), \tag{46}$$

which, according to (20), is equivalent to the so called *harmonic map heat flow* (HMH flow) into spheres

$$\mathbf{m}_t - \alpha_L \Delta\mathbf{m} = \alpha_L |\nabla\mathbf{m}|^2 \mathbf{m}, \quad \text{subject to } |\mathbf{m}| = 1, \tag{47}$$

equipped with the zero Neumann conditions and appropriate initial conditions.

Stability and convergence of several different finite element approximation schemes for harmonic maps was studied in [46].

3.5.1 Cross-Product Type Algorithm for HMH Flow

The study of (47) as the limit case of the LL equation for $\beta_L = 0$, is challenging because of the different nature of (47) and the LL equation (6). For the LL equation we have the equivalence with the LLG form and for the LLG form, we have successfully shown the convergence results for Algorithm 2. However, the proof of the convergence strongly relied on the actual form of the LLG equation. In the case of (46) we do not have any form similar to the LLG form. So when designing a finite element approach, we must depart directly from (46). The following scheme was proposed in [45].

Algorithm 4 *Given $\mathbf{m}^j \in V_h$ find $\mathbf{m}^{j+1} \in V_h$ such that for all $\phi \in V_h$ there holds*

$$(\delta\mathbf{m}^{j+1}, \phi)_h + \alpha_L(\mathbf{m}^{j+1/2} \times (\mathbf{m}^{j+1/2} \times \tilde{\Delta}_h \mathbf{m}^{j+1/2}), \phi)_h = 0. \tag{48}$$

We can directly see that the above mentioned scheme conserves the magnitude of $\mathbf{m}^j$ in the nodes of the mesh. Existence of a solution in each step of Algorithm 4 can be established with Brouwer's fixed point theorem independently of the discretization parameters. Since in practice the discrete scheme requires the solution or approximation of a nonlinear system of equations in each time step Prohl and Bartels [45] decided to analyze a larger class of schemes by allowing a (small) right-hand side with an appropriate vector product structure. They propose and analyze an iterative method, see Algorithm 5, for the approximation of the system of equations in (48) that converges provided that $\tau = o(h^2)$ and which introduces a residual that does not significantly influence the properties of discrete solutions.

So instead of solving (48) they suggest to solve the equation

$$(\delta\mathbf{m}^{j+1}, \phi)_h + \alpha_L(\mathbf{m}^{j+1/2} \times (\mathbf{m}^{j+1/2} \times \tilde{\Delta}_h \mathbf{m}^{j+1/2}), \phi)_h = (\mathbf{m}^{j+1/2} \times \mathbf{r}^{j+1}), \phi)_h, \tag{49}$$

for $\mathbf{r}^{j+1} \in V_h$ satisfying $\|\mathbf{r}^j\|_h \le \varepsilon$, where the role of typically small parameter ε is specified later in Algorithm 5.

Remark 12 The idea of introducing the residual with an appropriate vector product structure deserves an emphasis. As presented above, the idea was used for the harmonic map heat flow; however, it can be used also for the LL equation [44]. This approach elegantly overcomes the problem of fixed-point iterations from Algorithm 3. Originally, the steps from Algorithm 3 do not preserve the length of magnetization. So the effort made in order to design the norm preserving Algorithm 2 was actually degraded by the fact, that the nonlinear system was then solved by the norm nonconserving fixed-point iterations from Algorithm 3. For more details we refer to [44].

Provided we have the sequences $\{\mathbf{m}^j\}_{j=0,\dots,J}$ and $\{\mathbf{r}^j\}_{j=0,\dots,J}$ solving (49), the following result has been shown in [45].

Theorem 2 *Let τ and ε be positive numbers, and $(\mathcal{T}_h)_{h>0}$ be a family of regular triangulations of Ω with maximal mesh-size h. Suppose that* (i) $\mathbf{r}^i \in V_h$ *satisfies* $\|\mathbf{r}^i\|_h \le \varepsilon$, *for* $0 \le i \le J$, (ii) $|\mathbf{m}^0(z)| = 1$ *for all nodes* $z \in \mathcal{N}_h$, (iii) *for all* $0 \le i \le J-1$ *and for all* $\phi \in V_h$ *the relation* (49) *holds.*

Then the modulus of $\mathbf{m}^i$ is preserved, that is,

$$|\mathbf{m}^j(z)| = 1$$

for all nodes $z \in \mathcal{N}_h$ and for $0 \le i \le J$. If $J\tau > T$ and $\mathbf{m}^0 \to \mathbf{m}_0$ in $W^{1,2}(\Omega)$ for $h \to 0$ then, taking $\hat{\mathbf{m}}_{h,\tau,\varepsilon}$ as a piecewise linear approximation of $\mathbf{m}^i$, there exists a subsequence of $(\hat{\mathbf{m}}_{h,\tau,\varepsilon})$ as $(h,\tau,\varepsilon) \to 0$ which converges weakly in $W^{1,2}(\Omega_T)$ to a weak solution of the harmonic map heat flow problem.

To be exhaustive, we provide the definition of weak solution to the harmonic map heat flow problem, which is almost identical to the definition of weak solutions to the LL equation. The only difference is the relation (51).

Definition 2 Given $\mathbf{m}_0 \in W^{1,2}(\Omega)$ such that $|\mathbf{m}_0| = 1$ almost everywhere in Ω, a function $\mathbf{m}$ is called *a weak solution of harmonic heat flow problem* if for all positive T there holds (i) $\mathbf{m} \in H^1(\Omega_T, \mathbb{R}^3)$ with $\mathbf{m}(0,\cdot) = \mathbf{m}_0$ in the sense of traces, (ii) $|\mathbf{m}| = 1$ almost everywhere in Ω_T, (iii) for almost

all $T' \in (0,T)$ there holds

$$\frac{1}{2}\int_\Omega |\nabla \mathbf{m}(T',x)|^2 \mathrm{d}x + \alpha_L \int_0^{T'} \|\mathbf{m}_t\|_2^2 \mathrm{d}t \leq \frac{1}{2}\int_\Omega |\nabla \mathbf{m}_0(x)|^2 \mathrm{d}x, \tag{50}$$

and, (iv) for all $\phi \in C^\infty(\overline{\Omega}_T, \mathbb{R}^3)$ there holds

$$\int_0^T (\mathbf{m}_t, \mathbf{m}\times\phi)\mathrm{d}t + \alpha_L \int_0^T (\nabla \mathbf{m}, \nabla(\mathbf{m}\times\phi))\mathrm{d}t = 0. \tag{51}$$

Remark 13 The key ingredients of the proof of Theorem 2 are the approximation estimates (36)–(38). Thanks to them we can get rid of the troublesome terms including the second space derivatives. Of course, one has to pay for this, namely by the dependence of the time step τ on the space discretization step h. Notice, however, that this dependence does not involve the dimension of the domain. So all results are valid in 2D as well as in 3D.

The proof of the previous theorem is again threefold. The main steps are illustrated in Fig. 8. In the first step the following a priori estimates for the approximate solution are derived

$$\frac{1}{2}\|\nabla \mathbf{m}^{J'}\|_2^2 + (\alpha_L - \varepsilon)\tau \sum_{i=0}^{J'-1} \|\mathbf{m}^{i+1/2} \times \tilde{\Delta}_h \mathbf{m}^{i+1/2}\|_h^2 \leq \frac{1}{2}\|\nabla \mathbf{m}^0\|_2^2 + \frac{1}{4}J'\tau\varepsilon,$$

$$\frac{1}{2}\|\nabla \mathbf{m}^{J'}\|_2^2 + (\alpha_L - \varepsilon)^2\tau \sum_{i=0}^{J'-1} \|\delta \mathbf{m}^{i+1}\|_h^2 \leq \frac{1}{2}\|\nabla \mathbf{m}^0\|_2^2 + \frac{5}{4}J'\tau\varepsilon.$$

These estimates are obtained by different choices of test function in (49).

Then, using these a priori estimates, the existence is showed of a subsequence of $\{\hat{\mathbf{m}}_{h,\tau,\varepsilon}\}$ such that for $(h,\tau,\varepsilon) \to 0$ the following convergence results can be verified

$$\begin{aligned}
&\hat{\mathbf{m}}_t \rightharpoonup \mathbf{m}_t \quad \text{in } L^2(\Omega_T),\\
&\overline{\mathbf{m}} \to \mathbf{m} \quad \text{in } L^2(\Omega_T),\\
&\nabla\overline{\mathbf{m}} \rightharpoonup \nabla\mathbf{m} \quad \text{in } L^2(\Omega_T),\\
&\mathbf{m}^+ \rightharpoonup^* \mathbf{m} \quad \text{in } L^\infty((0,T), W^{1,2}(\Omega)).
\end{aligned}$$

Finally, we have to find out what $\mathbf{m}$ the sequence $\{\hat{\mathbf{m}}_{h,\tau,\varepsilon}\}$ is converging to. Departing from (49) it is possible to show by combining of the properties of $(\cdot,\cdot)_h$, $W^{1,2}(\Omega)$-stability of $\mathcal{I}_h$, convergence results mentioned above, and interpolation estimates (36)–(38) that $\mathbf{m}$, as a limit of $\{\hat{\mathbf{m}}_{h,\tau,\varepsilon}\}$, is a weak solution to the harmonic map heat flow problem.

Having the results on the convergence of Algorithm 4 it seems that all necessary work has been done. Unfortunately, Algorithm 4 involves the solution of a nonlinear system of the equations. One approach is to use the standard methods, such as Newton method or Broyden method. Disadvantage of this approach is that we loose the hardly obtained property of conservation of the modulus of $\mathbf{m}^j$. The classical iteration methods do not look at the structure of the problem. In the inner iterations, represented by, e.g., index l, would no more be valid that $|\mathbf{m}^{j+1,l+1}| = |\mathbf{m}^{j+1,l}|$.

Bartels and Prohl suggest a reasonable fast and reliable solver giving the sequences $\{\mathbf{m}^j\}_{j=0,\dots,J}$ and $\{\mathbf{r}^j\}_{j=0,\dots,J}$ satisfying the assumptions of the previous theorem and still, the modulus of magnetization in the inner iterations is preserved.

Algorithm 5 Input: *parameters* h,τ,ε,J *as from Theorem* 2, $\mathbf{m}^0 \in V_h$ *such that* $|\mathbf{m}^0(z)| = 1$ *for all nodes* $z \in \mathcal{N}_h$.

(a) *Set* $i = 0$, $\mathbf{r}^0 = 0$.
(b) *Set* $\mathbf{w}^{i+1,0} = \mathbf{m}^i$.
  (b1) *Set* $l = 0$.
  (b2) *Compute* $\mathbf{w}^{i+1,l+1} \in V_h$ *such that*

$$\begin{aligned}
&\frac{2}{\tau}(\mathbf{w}^{i+1,l+1},\phi)_h \\
&\quad + \alpha_L(\mathbf{w}^{i+1,l+1} \times (\mathbf{w}^{i+1,l} \times \tilde{\Delta}_h \mathbf{w}^{i+1,l}),\phi)_h \\
&\quad + \beta_L(\mathbf{w}^{i+1,l+1} \times \tilde{\Delta}_h \mathbf{w}^{i+1,l},\phi)_h \\
&= \frac{2}{\tau}(\mathbf{m}^i,\phi)_h,
\end{aligned} \tag{52}$$

  for all $\phi \in V_h$. *Set* $\mathbf{e}^{i+1,l+1} = \mathbf{w}^{i+1,l+1} - \mathbf{w}^{i+1,l}$ *and*

$$\begin{aligned}
\mathbf{r}^{i+1} = \alpha_L(&\mathbf{w}^{i+1,l+1} \times \tilde{\Delta}_h \mathbf{e}^{i+1,l+1} \\
&+ \mathbf{e}^{i+1,l+1} \times \tilde{\Delta}_h \mathbf{w}^{i+1,l}) + \beta_L \Delta \mathbf{e}^{i+1,l+1}.
\end{aligned}$$

  (b3) *Go to* (c) *if* $\|\mathbf{r}^{i+1}\|_h \leq \varepsilon$; *set* $l = l+1$ *and continue with* (b2) *otherwise.*
(c) *Set* $\mathbf{m}^{i+1} = 2\mathbf{w}^{i+1,l+1} - \mathbf{m}^i$.
(d) *Stop if* $i+1 = J$; *set* $i = i+1$ *and go to* (b) *otherwise.*

Output: *Sequences* $(\mathbf{m}^i)_{i=0,\dots,J}$ *and* $(\mathbf{r}^i)_{i=0,\dots,J}$.

Remark 14 *The efficiency* of the method is guaranteed by the clever choice of a unknown $\mathbf{w}^{j+1,l+1}$ in (52). Without introducing $\mathbf{w}^{j+1,l+1}$, the equation (52) would have contained far more terms due to the cross-product structure with three terms. When using $\mathbf{w}^{j+1,l+1}$, which actually approximates the quantity $\mathbf{m}^{j+1/2}$, one gets only few terms when assembling the matrix of the final linear system.

The reliability of the presented algorithm is verified first by checking if all steps in Algorithm 5 are well-defined. This

can be seen by realizing that the left-hand side of (52) defines a continuous bilinear form. The ellipticity of the bilinear form can be shown by the choice of the test function $\phi = \mathbf{w}^{j+1,l+1}$.

Further, subtracting two subsequent equations in (b2), choosing $\phi = e^{(j+1,l+1)}$, and using the approximation estimates (36)–(38), leads to

$$\|\mathbf{e}^{j+1,l+1}\|_h \leq c_1 \tau h^{-2} \|\mathbf{e}^{j+1,l}\|_h,$$

which is valid for $l \geq 1$. Choosing $\tau < c_1^{-1} h^2$ ensures that $\|\mathbf{r}^{j+1}\|_h$, defined in (b2), will eventually descend under the beforehand known ε.

Finally, it is necessary to verify that $\mathbf{m}^{j+1}$ defined in (c) actually satisfies (49), which is only a straightforward computation.

3.5.2 Lagrange Multipliers for HMH Flow

A different convergent discretization for the HMH flow problem (47) was introduced in [47]. The authors use approximate discrete Lagrange multipliers. To motivate their approach, recall that to describe the gradient flow for energy requires mappings $\mathbf{m} : \Omega_T \to \mathbb{R}^m$, and a Lagrange multiplier $\lambda : \Omega_T \to \mathbb{R}^+$, such that

$$\mathbf{m}_t - \Delta \mathbf{m} = \lambda \mathbf{m} \quad \text{and} \quad |\mathbf{m}| = 1 \quad \Omega_T,$$

where coefficient α_L from (47) is taken to be equal one. In fact $\lambda = |\nabla \mathbf{m}|^2$.

The authors propose a scheme using an *approximate discrete* Lagrange multiplier to enforce both the discrete sphere constraint, i.e., unit length of (iterates of) finite element functions at nodes of a triangulation $\mathcal{T}_h$, and a discrete energy law.

Algorithm 6 *For $n \geq 0$, let $\mathbf{m}^j \in V_h$ be given, and find $\mathbf{m}^{j+1}, \lambda^{j+1} \in (V_h, V_h)$, such that for all $\phi \in V_h$ and for all $z \in \mathcal{N}_h$ there holds*

$$(\delta \mathbf{m}^{j+1}, \phi)_h + (\nabla \mathbf{m}^{j+1/2}, \nabla \phi) = (\lambda^{j+1} \mathbf{m}^{j+1/2}, \phi)_h, \tag{53}$$

$$\lambda^{j+1}(z) = \begin{cases} 0 & \text{if } \mathbf{m}^{j+1/2}(z) = 0, \\ \frac{(\nabla \mathbf{m}^{j+1/2}, \nabla(\mathbf{m}^{j+1/2}(z)\varphi_z))}{\beta_z |\mathbf{m}^{j+1/2}(z)|^2} & \text{else.} \end{cases} \tag{54}$$

Notice, that the actual explicit expression for λ^{j+1} is chosen in such a way that the discrete sphere constraint $|\mathbf{m}^{j+1}(z)| = 1$ is satisfied. This expression comes from the equality obtained when $\phi = \mathbf{m}^{j+1/2}(z)\varphi_z$ is put into (53). The parameter β_z is from the definition of reduced integration, see (34) and φ_z are the Lagrange finite element base functions defined in Sect. 3.2.

The well-posedness of the Algorithm 6 is verified under the condition $\tau = \mathcal{O}(h^2)$ for quasi-uniform meshes consisting of triangles in 2D and tetrahedra in 3D. The system is nonlinear and Brouwer's fixed-point theorem was used to prove the existence of solutions on every time level satisfying (53)–(54) and discrete versions of the sphere constraint and the energy law.

From the just obtained sequence $\{\mathbf{m}^j\}$ one can form piecewise constant and piecewise linear approximations in time domain $\overline{\mathbf{m}}_{\tau,h}(t), \mathbf{m}^+_{\tau,h}(t)$ and $\hat{\mathbf{m}}_{\tau,h}(t)$ which are now (τ, h)-dependent. Finally, from discrete versions of the sphere constraint and the energy law one can verify weak (sub)convergence of $\{\mathbf{m}_{\tau,h}\}$ to the weak solutions of HMH flow.

3.5.3 p-harmonic Flow

The idea of cross-product type schemes can be applied also for the p-harmonic flow into spheres governed by the following equation

$$\mathbf{u}_t - \Delta_p \mathbf{u} = |\nabla \mathbf{u}|^p \mathbf{u}, \tag{55}$$

with the same side-constraints and boundary conditions as for the harmonic map heat flow (47). Here, $\Delta_p \mathbf{u} = \nabla \cdot (|\nabla \mathbf{u}|^{p-2} \nabla \mathbf{u})$, where $1 < p < \infty$. Special choice $p = 2$ gives the harmonic map heat flow.

We have already pointed out in Remark 9 that the AJ scheme defined in Algorithm 1 can be adapted also for the case of the p-harmonic map heat flow [43]. An another approach, using the idea of cross-product type schemes, departs from the following form of governing equation, which is equivalent to (55)

$$\mathbf{u}_t - \mathbf{u} \times (\mathbf{u} \times \Delta_p \mathbf{u}) = 0.$$

The discretization of the previous equation leads to the similar algorithm to Algorithm 4. For further details on the analysis of such a scheme we refer to [48].

3.6 Cross-Product Type Schemes—LL Form

Although for the LL equation there exist two forms, the LL form and the LLG form, all schemes from Sects. 3.3, 3.4 dealing with weak solutions, are based on the discretization of the LLG form. There is however at least one good reason why to study and to prove the convergence results for the mid-point rule scheme derived directly from the LL form and focus not only on schemes derived from the LLG form:

Study of the limit process $\beta_L \to 0$. Algorithm 2 is not suitable for the study of a sequence of the problems for decreasing values of β_L to zero. Indeed, for $\beta_L \to 0$ we get $\alpha_G \to \infty$ and $\beta_G \to \infty$ and thus the time step in Algorithm 2 must go to zero, which is impossible. On the other

hand, Algorithm 7 behaves normally, no refinement of the time discretization is needed for $\beta_L \to 0$. The only effect is that the influence of the term $\mathbf{m} \times \Delta \mathbf{m}$ vanishes.
Moreover, taking Algorithm 7 and setting $\beta_L = 0$ we get directly Algorithm 4 by which we see a natural link between the LL equation and the harmonic map heat flow.

Motivated by the works on the constraint-preserving mid-point rule derived from the LLG form [11] and by the scheme for harmonic map heat flow [45] we obtained similar convergence results for a mid-point finite element scheme derived directly from the LL form. The algorithm reads as

Algorithm 7 *Given* $\mathbf{m}^j \in V_h$ *and* $\mathbf{r}^j$ *satisfying*

$$\|\mathbf{r}^j\|_h \le \varepsilon$$

find $\mathbf{m}^{j+1} \in V_h$ *such that for all* $\phi \in V_h$ *there holds*

$$\begin{aligned}(\delta\mathbf{m}^{i+1}, \phi)_h &+ \alpha_L(\mathbf{m}^{i+1/2} \times (\mathbf{m}^{i+1/2} \times \tilde{\Delta}_h \mathbf{m}^{i+1/2}), \phi)_h \\ &+ \beta_L(\mathbf{m}^{i+1/2} \times \tilde{\Delta}_h \mathbf{m}^{i+1/2}, \phi)_h \\ &= (\mathbf{m}^{i+1/2} \times \mathbf{r}^{j+1}, \phi)_h. \end{aligned} \tag{56}$$

We call this scheme Bartels-Prohl scheme for the LL form, see Table 1 for comparison with other schemes.

For this algorithm it was proved the same theorem as is Theorem 2, except that the validity of (56) is required instead of (49).

Theorem 3 *Let* τ *and* ε *be positive numbers, and* $(\mathcal{T}_h)_{h>0}$ *be a family of regular triangulations of* Ω *with maximal mesh-size* h. *Suppose that* (i) $\mathbf{r}^i \in V_h$ *satisfies* $\|\mathbf{r}^i\|_h \le \varepsilon$, *for* $0 \le i \le J$, (ii) $|\mathbf{m}^0(z)| = 1$ *for all nodes* $z \in \mathcal{N}_h$, (iii) *for all* $0 \le i \le J-1$ *and for all* $\phi \in V_h$ *the relation* (56) *holds.*
Then the modulus of $\mathbf{m}^i$ *is preserved, that is,*

$$|\mathbf{m}^j(z)| = 1$$

for all nodes $z \in \mathcal{N}_h$ *and for* $0 \le i \le J$. *If* $J\tau > T$ *and* $\mathbf{m}^0 \to \mathbf{m}_0$ *in* $W^{1,2}(\Omega)$ *for* $h \to 0$ *then, taking* $\hat{\mathbf{m}}_{h,\tau,\varepsilon}$ *as a piecewise linear approximation of* $\mathbf{m}^i$, *there exists a subsequence of* $(\hat{\mathbf{m}}_{h,\tau,\varepsilon})$ *as* $(h, \tau, \varepsilon) \to 0$ *which converges weakly in* $W^{1,2}(\Omega_T)$ *to a weak solution of the LL equation.*

The proof of the previous theorem relies basically on the same arguments as the proof of Theorem 2 from [45], see also Fig. 8. However, it requires more careful interplay between the constants, since in [45] the authors consider α_L being equal to one and on some places of the proof they make use of the fact, that $\alpha_L^2 = \alpha_L$ for $\alpha_L = 1$.

As we already pointed out, the scheme (56), suffers from the nonlinearity. In Theorem 3 we have stated the conservation of the modulus $|\mathbf{m}^i|$ for (56). Next we complete our analysis by suggesting how to solve (56) on one time level. We adapt Algorithm 5 for the harmonic map heat flow problem according to our needs.

Algorithm 8 Input: *parameters* h, τ, ε, J *as from Theorem 3,* $\mathbf{m}^0 \in V_h$ *such that* $|\mathbf{m}^0(z)| = 1$ *for all nodes* $z \in \mathcal{N}_h$.

(a) *Set* $i = 0$, $\mathbf{r}^0 = 0$.
(b) *Set* $\mathbf{w}^{i+1,0} = \mathbf{m}^i$.
  (b1) *Set* $l = 0$.
  (b2) *Compute* $\mathbf{w}^{i+1,l+1} \in V_h$ *such that*

$$\begin{aligned}&\frac{2}{\tau}(\mathbf{w}^{i+1,l+1}, \phi)_h \\ &\quad + \alpha_L(\mathbf{w}^{i+1,l+1} \times (\mathbf{w}^{i+1,l} \times \tilde{\Delta}_h \mathbf{w}^{i+1,l}), \phi)_h \\ &\quad + \beta_L(\mathbf{w}^{i+1,l+1} \times \tilde{\Delta}_h \mathbf{w}^{i+1,l}, \phi)_h = \frac{2}{\tau}(\mathbf{m}^i, \phi)_h,\end{aligned}$$

  for all $\phi \in V_h$. *Set* $\mathbf{e}^{i+1,l+1} = \mathbf{w}^{i+1,l+1} - \mathbf{w}^{i+1,l}$ *and*

$$\begin{aligned}\mathbf{r}^{i+1} = \alpha_L(&\mathbf{w}^{i+1,l+1} \times \tilde{\Delta}_h \mathbf{e}^{i+1,l+1} \\ &+ \mathbf{e}^{i+1,l+1} \times \tilde{\Delta}_h \mathbf{w}^{i+1,l}) + \beta_L \tilde{\Delta}_h \mathbf{e}^{i+1,l+1}.\end{aligned}$$

  (b3) *Go to* (c) *if* $\|\mathbf{r}^{i+1}\|_h \le \varepsilon$; *set* $l = l+1$ *and continue with* (b2) *otherwise.*
(c) *Set* $\mathbf{m}^{i+1} = 2\mathbf{w}^{i+1,l+1} - \mathbf{m}^i$.
(d) *Stop if* $i + 1 = J$; *set* $i = i + 1$ *and go to* (b) *otherwise.*

Output: *Sequences* $(\mathbf{m}^i)_{i=0,\dots,J}$ *and* $(\mathbf{r}^i)_{i=0,\dots,J}$.

We can say the same about the reliability and the efficiency of Algorithm 8 as we have said for Algorithm 5 in Remark 14.

3.7 Cross-Product Type Scheme for Coupled Maxwell-LL System

The program elaborated in Sects. 3.4–3.6 was successfully extended and applied in [10] for the coupled Maxwell-Landau-Lifshitz system (10)–(12) introduced in Sect. 1.4.1. Following the cross-product type schemes, one can suggest a, for the reader already familiar, discretization of the LL part analogical to (42). For the electric and magnetic part of the M-LL system we use the discretization from [9]. Denote by X_h and Y_h finite element spaces approximating the functions spaces of $\mathbf{E}$ and H. Both finite element spaces must be chosen such that $X_h \subset H_0(\mathbf{curl}, \Omega^{\text{out}})$, $Y_h \subset L^2(\Omega^{\text{out}})$ and $\nabla \times X_h \subset Y_h$. Note, that for the M-LL system we work on a setting of two domains Ω and Ω^{out} such that $\Omega \Subset \Omega^{\text{out}}$, see the description of the M-LL system from Sect. 1.4.1. Complete discrete system reads as follows.

Algorithm 9 *Let* $(\mathbf{m}^0, \mathbf{E}^0, \mathbf{H}^0) \in V_h \times X_h \times Y_h$. *For* $J \ge 0$ *and* $(\mathbf{m}^j, \mathbf{E}^j, \mathbf{H}^j) \in V_h \times X_h \times Y_h$ *let* $(\mathbf{m}^{j+1}, \mathbf{E}^{j+1}, \mathbf{H}^{j+1}) \in$

$V_h \times X_h \times Y_h$ solve

$$(\delta \mathbf{m}^{j+1}, \phi)_h + \alpha(\mathbf{m}^j \times \delta \mathbf{m}^{j+1}, \phi)_h = (1+\alpha^2)(\mathbf{m}^{j+1/2} \times (\tilde{\Delta}_h \mathbf{m}^{j+1/2} + P_{V_h}\mathbf{H}^{j+1/2}), \phi)_h \quad \text{for all } \phi \in V_h, \tag{57}$$

$$\varepsilon_0(\delta \mathbf{E}^{j+1}, \varphi) - (\mathbf{H}^{j+1/2}, \nabla \times \varphi) + \sigma(\chi_\Omega \mathbf{E}^{j+1/2}, \varphi) = -(\mathbf{J}^{j+1/2}, \varphi) \quad \text{for all } \varphi \in X_h, \tag{58}$$

$$\mu_0(\delta \mathbf{H}^{j+1}, \zeta) + (\nabla \times \mathbf{E}^{j+1/2}, \zeta) = -\mu_0(\mathbf{m}_t^{j+1}, \zeta) \quad \text{for all } \zeta \in Y_h. \tag{59}$$

Here, $P_{V_h} : L^2(\Omega) \to V_h$, with $(P_{V_h}\mathbf{u}, \phi)_h = (u, \phi)$ for all $\phi \in V_h$ denotes the L^2-projection into V_h.

Finite element spaces X_h and Y_h are defined according to [49, Chap. 8] as Nédelec's first and second family of edge elements on tetrahedrons

$$X_h = \{\varphi \in H_0(\mathbf{curl}, \Omega^{\text{out}}) : \varphi|_K \in \mathcal{P}_1(K, \mathbb{R}^3), \text{ for all } K \in \mathcal{T}_h\},$$

and

$$Y_h = \{\zeta \in L^2(\Omega^{\text{out}}) : \zeta|_K \in \mathcal{P}_0(K, \mathbb{R}^3), \text{ for all } K \in \mathcal{T}_h\}.$$

For the above edge elements spaces, the following global interpolants of sufficiently smooth functions ($\delta > 0$, $p > 2$) are available

$$\mathcal{I}_{X_h} : W^{1/2+\delta,2}(\Omega^{\text{out}}) \cap W^{1,p}(\Omega^{\text{out}}) \to X_h,$$

and

$$\mathcal{I}_{Y_h} : W^{1/2+\delta,2}(\Omega^{\text{out}}) \to Y_h.$$

They satisfy the following interpolation properties

$$\|\varphi - \mathcal{I}_{X_h}\varphi\|_2 + h\|\nabla \times (\varphi - \mathcal{I}_{X_h}\varphi)\|_2 \le Ch^2\|\nabla^2\varphi\|_2,$$
$$\|\zeta - \mathcal{I}_{Y_h}\zeta\|_2 \le Ch\|\zeta\|_{W^{1,2}}.$$

In order to have a consistent set of initial conditions which satisfy the physical constraint $\nabla \cdot B_0 = 0$, we require

$$\begin{aligned} &\nabla \cdot (\mathbf{H}_0 + \chi_\Omega \mathbf{m}_0) = 0 \quad \text{in } \Omega^{\text{out}}, \\ &\langle \mathbf{H}_0 + \chi_\Omega \mathbf{m}_0, \mathbf{n} \rangle = 0 \quad \text{on } \partial\Omega^{\text{out}}, \end{aligned} \tag{60}$$

where $\mathbf{n}$ is the outer unit normal to the boundary of Ω^{out}. We assume the initial data satisfy

$$\mathbf{m}_0 \in W^{1,2}(\Omega), \qquad \mathbf{H}_0, \mathbf{E}_0 \in L^2(\Omega^{\text{out}}), \qquad \mathbf{J} \in L^2(\Omega^{\text{out}}). \tag{61}$$

We provide the definition of a weak solution to the M-LL system.

Definition 3 Suppose (60) and (61). Then $(\mathbf{m}, \mathbf{E}, \mathbf{H})$ is called weak solution to the Maxwell-LL system, if for all positive T there holds (i) $\mathbf{m} \in L^\infty(0, T; W^{1,2}(\Omega))$, such that $\mathbf{m}_t \in L^2(\Omega_T)$ with $\mathbf{m}(0, \cdot) = \mathbf{m}_0$ in sense of traces, and $\mathbf{E}, \mathbf{H} \in L^\infty(0, T; L^2(\Omega))$, (ii) $|\mathbf{m}| = 1$ almost everywhere in Ω_T, (iii) for almost all $T' \in (0, T)$ there holds

$$\mathcal{E}_{(\mathbf{m},\mathbf{E},\mathbf{H})}(T') + \int_{\Omega_{T'}} \left(\frac{\alpha\mu_0}{1+\alpha^2}|\mathbf{m}_t|^2 + \sigma|\mathbf{E}|^2 \right) \mathrm{d}\mathbf{x}\,\mathrm{d}t \le \mathcal{E}_{(\mathbf{m},\mathbf{E},\mathbf{H})}(0) - \int_{\Omega^{\text{out}}_{T'}} (\mathbf{J}, \mathbf{E}) \mathrm{d}\mathbf{x}\,\mathrm{d}t,$$

where

$$\mathcal{E}_{(\mathbf{m},\mathbf{E},\mathbf{H})}(T') = \frac{\mu_0}{2}\int_\Omega |\nabla \mathbf{m}(T', \cdot)|^2 \mathrm{d}\mathbf{x} + \int_{\Omega^{\text{out}}} \left[\frac{\mu_0}{2}|\mathbf{H}(T', \cdot)|^2 + \frac{\varepsilon_0}{2}|\mathbf{E}(T', \cdot)|^2 \right] \mathrm{d}\mathbf{x}$$

and, (iv) for all $\phi \in C^\infty(\overline{\Omega})$, and $\zeta \in \mathcal{D}([0, T); C^\infty(\Omega^{\text{out}}) \cap H_0(\mathbf{curl}, \Omega^{\text{out}}))$ there holds

$$\begin{aligned} &\int_{\Omega_T} \langle \mathbf{m}_t, \phi \rangle \mathrm{d}\mathbf{x}\,\mathrm{d}t + \alpha \int_{\Omega_T} \langle \mathbf{m} \times \mathbf{m}_t, \phi \rangle \mathrm{d}\mathbf{x}\,\mathrm{d}t \\ &= -(1+\alpha^2)\left[\int_{\Omega_T} \langle \mathbf{m} \times \nabla \mathbf{m}, \nabla \phi \rangle \mathrm{d}\mathbf{x}\,\mathrm{d}t - \int_{\Omega_T} \langle \mathbf{m} \times \mathbf{H}, \phi \rangle \mathrm{d}\mathbf{x}\,\mathrm{d}t \right], \end{aligned} \tag{62}$$

$$\begin{aligned} &-\varepsilon_0 \int_{\Omega^{\text{out}}_T} \langle \mathbf{E}, \zeta_t \rangle \mathrm{d}\mathbf{x}\,\mathrm{d}t - \int_{\Omega^{\text{out}}_T} \langle \mathbf{H}, \nabla \times \zeta \rangle \mathrm{d}\mathbf{x}\,\mathrm{d}t + \sigma \int_{\Omega_T} \langle \mathbf{E}, \zeta \rangle \mathrm{d}\mathbf{x}\,\mathrm{d}t \\ &= -\int_{\Omega^{\text{out}}_T} \langle \mathbf{J}, \zeta \rangle \mathrm{d}\mathbf{x}\,\mathrm{d}t + \varepsilon_0 \int_{\Omega^{\text{out}}} \langle \mathbf{E}_0, \zeta(0, \cdot) \rangle \mathrm{d}\mathbf{x}, \end{aligned} \tag{63}$$

$$\begin{aligned} &-\mu_0 \int_{\Omega^{\text{out}}_T} \langle \mathbf{H} + \chi_\Omega \mathbf{m}, \zeta_t \rangle \mathrm{d}\mathbf{x}\,\mathrm{d}t + \int_{\Omega^{\text{out}}_T} \langle \mathbf{E}, \nabla \times \zeta \rangle \mathrm{d}\mathbf{x}\,\mathrm{d}t \\ &= \mu_0 \int_{\Omega^{\text{out}}} \langle \mathbf{H}_0, \zeta(0, \cdot) \rangle \mathrm{d}\mathbf{x} + \mu_0 \int_\Omega \langle \mathbf{m}_0, \zeta(0, \cdot) \rangle \mathrm{d}\mathbf{x}. \end{aligned} \tag{64}$$

Existence of weak solutions has first been shown in [50].

The convergence result is summarized in the following theorem. The proof basically follows the three-step procedure depicted in Fig. 8, for more details we refer to [10].

Theorem 4 *Let (60) and (61) be valid. Let τ be a positive number, and $(\mathcal{T}_h)_{h>0}$ be a family of regular triangulations of Ω^{out} with maximal mesh-size h. Suppose that* (i) $|\mathbf{m}^0(z)| =$

1 *for all nodes* $z \in \mathcal{N}_h$, (ii) *for all* $0 \le i \le J-1$ *and for all* $\phi \in V_h, \varphi \in X_h, \zeta \in Y_h$ *the relations* (57)–(59) *hold.*

Then the modulus of $\mathbf{m}^i$ *is preserved, that is,*

$$|\mathbf{m}^j(z)| = 1$$

for all nodes $z \in \mathcal{N}_h$ *and for* $0 \le i \le J$. *For* $J\tau > T$ *assume* $\mathbf{m}^0 \to \mathbf{m}_0$ *in* $W^{1,2}(\Omega)$ *and* $(\hat{\mathbf{H}}^0, \hat{\mathbf{E}}^0) \to (\mathbf{H}^0, \mathbf{E}^0)$ *in* $L^2(\Omega^{\text{out}})$ *for* $h \to 0$ *such that* (60) *is fulfilled, and fix* $T > 0$. *Then, taking* $(\hat{\mathbf{m}}, \hat{\mathbf{E}}, \hat{\mathbf{H}})_{\tau,h}$ *as a piecewise linear approximation of* $(\mathbf{m}^i, \mathbf{E}^i, \mathbf{H}^i)$ *there exists a subsequence of* $(\hat{\mathbf{m}}, \hat{\mathbf{E}}, \hat{\mathbf{H}})_{\tau,h}$ *as* $(h, \tau) \to 0$ *which converges weakly* to* $(\mathbf{m}, \mathbf{E}, \mathbf{H})$ *in*

$$[L^\infty(0,T; W^{1,2}(\Omega^{\text{out}})) \cap W^{1,2}(\Omega_T)] \times [L^\infty(0,T; L^2(\Omega^{\text{out}}))]^2,$$

and $(\mathbf{m}, \mathbf{E}, \mathbf{H})$ *is a weak solution of the M-LL system.*

Baňas, Bartels and Prohl suggest a fixed-point iteration to solve the nonlinear system arising in Algorithm 9. The iterations are analogical to the ones appearing in Algorithms 5 and 8: Given $\mathbf{m}^j, \mathbf{H}^j, \mathbf{E}^j$ they aim at approximating $\mathbf{w} := \mathbf{m}^{j+1/2}, \mathbf{F} := \mathbf{E}^{j+1/2}, \mathbf{G} := \mathbf{H}^{j+1/2}$. The time derivative $\delta\mathbf{m}^{j+1}$ is replaced by $\frac{2}{\tau}(\mathbf{w} - \mathbf{m}^j)$ and similar expressions for $\delta\mathbf{E}^{j+1}$ and $\delta\mathbf{H}^{j+1}$. A linearization of the nonlinear term $\mathbf{w} \times (\tilde{\Delta}_h \mathbf{w} + P_{L^2}\mathbf{G}), \phi)_h$ and the identity $\mathbf{m}^j \times \delta\mathbf{m}^{j+1} = -\frac{2}{\tau}\mathbf{m}^{j+1/2} \times \mathbf{m}^j$ lead to the following algorithm.

Algorithm 10 Input: *parameters* τ, h, J, ε.

(a) *Set* $(\mathbf{w}^0, \mathbf{F}^0, \mathbf{G}^0) := (\tilde{\mathbf{m}}^j, \tilde{\mathbf{E}}^j, \tilde{\mathbf{H}}^j)$ *and* $l = 0$.

(b) *Compute* $(\mathbf{w}^{l+1}, \mathbf{F}^{l+1}, \mathbf{G}^{l+1}) \in V_h \times X_h^0 \times Y_h$ *such that for all* $(\phi, \varphi, \zeta) \in V_h \times X_h^0 \times Y_h$ *there holds*

$$\frac{2}{\tau}(\mathbf{w}^{l+1}, \phi)_h - \frac{2\alpha}{\tau}(\mathbf{w}^{l+1} \times \mathbf{m}). \tag{65}$$

(c) *Stop and set*

$$(\tilde{\mathbf{m}}^{j+1}, \tilde{\mathbf{E}}^{j+1}, \tilde{\mathbf{H}}^{j+1}) := 2(\mathbf{w}^{l+1}, \mathbf{F}^{l+1}, \mathbf{G}^{l+1}) - (\tilde{\mathbf{m}}^j, \tilde{\mathbf{E}}^j, \tilde{\mathbf{H}}^j),$$

once

$$\|\tilde{\Delta}_h(\mathbf{w}^{l+1} - \mathbf{w}^l)\|_h + \|\mathbf{G}^{l+1} - \mathbf{G}^l\|_2 \le \varepsilon.$$

(d) *Set* $l = l + 1$ *and go to* (b).

Output: *Triple* $(\tilde{\mathbf{m}}^{j+1}, \tilde{\mathbf{E}}^{j+1}, \tilde{\mathbf{H}}^{j+1})$.

For $\varepsilon \to 0$, the output of the iteration converges to the solution of (57)–(59) provided that $(\tilde{\mathbf{m}}^j, \tilde{\mathbf{E}}^j, \tilde{\mathbf{H}}^j) = (\mathbf{m}^j, \mathbf{E}^j, \mathbf{H}^j)$, and that $\tau \le Ch_{\min}^2/(1+\alpha^2)$ with a factor $c > 0$ that only depends on the geometry of $\mathcal{T}_h$.

Remark 15 The *efficiency* of the method is again guaranteed by the clever choice of unknowns $\mathbf{w}^{j+1}, \mathbf{F}^{j+1}$ and $\mathbf{G}^{j+1}$. The introduction of these unknowns rapidly decreases the number of terms to be assembled into the matrix of the final linear system.

The *reliability* of the method is controlled by the number $\Theta = c_1\|\tilde{\mathbf{m}}^j\|_\infty\sqrt{15}(1+\alpha^2)\tau h_{\min}^2$. It can be shown that the L^2-difference of two subsequent iterations in Algorithm 10 decreases with factor Θ. Thus one needs to keep $\Theta < 1$.

4 Computational Studies

We provide three computational studies of methods presented in Sects. 2–3. First, we take over the results of Baňas [51]. The computations were performed for the schemes from Sect. 2 and for semi-implicit schemes.

Second, we show the results of the cross-product type schemes for single LL equation from Sects. 3.3–3.6. Finally we present a numerical study of the coupled Maxwell-LL system from Sect. 3.7 taken over from [10].

4.1 Eddy Currents and the LL Equation without the Exchange Field

Consider a conducting thin film subjected to an in-plane circularly polarized magnetic field. This numerical example was also suggested in [52]. The problem can be reduced to a 1D problem on the interval $(0, \delta)$ where δ is the thickness of the film. In order to obtain the magnetic field $\mathbf{H} = (H_1, H_2, H_3)$, the LLG equation has to be coupled with the following eddy current equation

$$\mu_0 H_{it} - \frac{1}{\sigma} H_{izz} = -\mu_0 m_{it}, \quad \text{for } i = 1, 2, \tag{66}$$

and $H_3 = -m_3$, equipped with boundary condition

$$\mathbf{H}(t) = H_s(\cos(\omega t), \sin(\omega t), 0), \quad z = 0,\ z = \delta.$$

Here, μ_0 denotes the permeability and σ the conductivity of vacuum.

The LL equation, written using coefficients with good physical meaning, reads as

$$\mathbf{m}_t = -\gamma M_s(\mathbf{m} \times \mathbf{H}_{\text{eff}} + \alpha\mathbf{m} \times (\mathbf{m} \times \mathbf{H}_{\text{eff}})), \tag{67}$$

where γ is the gyromagnetic ratio, α denotes the damping parameter, M_s stands for the magnetization saturation. The link with original formulation (6) is expressed by $\beta_L = \gamma M_s$ and $\alpha_L = \alpha\gamma M_s$.

For the coupled system (66)–(67) we consider the effective field to be of the form

$$\mathbf{H}_{\text{eff}} = \frac{\mathbf{H}}{M_s} + \frac{2A_{\text{exc}}}{\mu_0 M_s^2}\mathbf{m}_{zz},$$

where A_{exc} is the exchange constant from (2).

Example 2 For the above described model consider the following parameters $\gamma = 2.211 \times 10^5$, $\alpha = 0.01$, $M_s = 8 \times 10^5$, $\sigma = 4 \times 10^6$, $\delta = 1.5 \times 10^{-6}$, $A_{\text{exc}} = 1.05 \times 10^{-11}$, $\omega = 2\pi \times 10^9$, $H_s = 4.5 \times 10^3$, $\mu_0 = 4\pi \times 10^{-7}$. A uniform initial condition for the LL equation is used $\mathbf{m}_0 = (1, 0, 0)$.

Methods to be compared are the following: Semi-implicit scheme (31) combined with the projection back onto sphere, classical mid-point scheme (29), extrapolated classical mid-point scheme (30), semi-implicit scheme with exact formula on one time level departing from Lemma 1, and the classical Runge-Kutta method of the fourth order.

In computational experiments, first the mesh parameter $h = \delta/50$ was fixed and the largest time step $\tau_{\max}$ was determined, for which an acceptable numerical solution without oscillations could be computed. Then, the value of h was decreased to see if the stability of the method was sensitive to the mesh refinement.

The main outcome of the computations is the following:

Although the performance of the methods for the LL equation is influenced by the coupling with (66), the errors induced by the discretization of (66) have minor influence on the computation, when compared to the effect of the discretization of the LL equation.

The only scheme for which the choice of the time step was independent of the mesh parameter h, was the semi-implicit scheme (31) with projection back onto sphere. However, the projection back onto sphere was essential to obtain this stability. Experiments without projection back onto sphere showed that the numerical approximation blows up for grater values of τ. Thus from all tested schemes, the above mentioned scheme is most suitable for the problems including the mesh adaptivity.

4.2 Blow-up Simulation of the LL Equation with Cross-Product Type Schemes

We present the results from [42] and from [11] focusing on singularity formation of (6). The formulation (9) shows that static solutions of the LL equation are exactly those of the harmonic map heat flow. So we prescribe the following initial condition motivated from the construction of the Struwe solution carried out in [35].

Example 3 Let $\mathbb{R}^2 \supset \Omega = (-1/2, 1/2)^2$, and let $\beta_L = -1$. Further define $\mathbf{m}_0 : \Omega \to S^2$ by

$$\mathbf{m}_0(\mathbf{x}) = \begin{cases} (0, 0, -1) & \text{for } |\mathbf{x}| \geq 1/2, \\ (2\mathbf{x}A, A^2 - |\mathbf{x}|^2)/(A^2 + |\mathbf{x}|^2) & \text{for } |\mathbf{x}| \leq 1/2, \end{cases}$$

where $A := (1 - s|\mathbf{x}|)^4/s$ for some $s > 0$. The triangulations $\mathcal{T}_l$ used in the numerical simulations are defined through a positive integer l and consist of 2^{2l+1} halved squares with edge length $h = 2^{-l}$. As discrete initial data we employed the nodal interpolant of $\mathbf{m}_0$.

In [42] the authors ran Algorithm 1 where instead of standard explicit L^2 integration they use reduced integration in order to improve the performance of the algorithm. They used

$$\tau = 0.1h^{5/2}(1 + \alpha_L^2)/\alpha_L,$$

following requirement mentioned in Remark 8.

The same example was computed by Algorithm 3 in [11]. In this computational study a relation

$$\tau = 0.1h^2(1 + \alpha_L^2)$$

was used.

Both algorithms were run with $s = 1, l = 4$, and $\alpha_L = 1,\ 1/4$. Figure 9 shows snapshots of the numerical solution for $\alpha_L = 1$ at various times. The plots in Fig. 9 display the orthogonal projection of the vector field $\mathbf{m}$ onto the plane xy. Observe that for $t \approx 0.0529$ the vector $\mathbf{m}(0.0529, \mathbf{0})$ changes its direction from $(1, 0, 0)$ to $(-1, 0, 0)$. Figure 10 magnifies this change of direction. For the smaller α_L the vector at the origin changes its direction at a significantly later time.

The following observations result from the comparison of both simulations.

Stabilizing effect of reduced integration. Primal observation is that the relation $\tau \sim h^2$ is not sufficient to guarantee stability and convergence of Algorithm 1. The results show that reduced integration stabilizes the scheme. Moreover, reduced integration significantly increased the efficiency of Algorithm 1, e.g., the CPU time is decreased by 90%.

Behavior for $h \to 0$. For fixed $\alpha_L = 1$ and $s = 4$ the space discretization was refined putting $l = 4, 5, 6$. In Fig. 11 the energy

$$E(\mathbf{m}(t)) = \frac{1}{2}\int_\Omega |\nabla \mathbf{m}(t, \cdot)|^2 d\mathbf{x},$$

and the $W^{1,\infty}$ semi-norm $\|\nabla \mathbf{m}\|_{L^\infty\Omega}$ are displayed as functions of t for $t \in (0, 6/100)$ for $l = 4,\ 5,\ 6$. For each $l = 4,\ 5,\ 6$, the function $t \to \|\nabla \mathbf{m}\|_{L^\infty\Omega}$ assumes the maximum value $2\sqrt{2}h^{-1}$ (among functions $\phi_h \in V_h$ with $|\phi_h| = 1$ for all nodes). We observe that for decreasing mesh-size h, the blow-up time (the time at which $\|\nabla \mathbf{m}\|_{L^\infty\Omega}$ assumes its maximum) approaches $t \approx 0.03$.

Dependence of blow-up time on α_L. In order to study the dependence of blow-up behavior on the parameter α_L, both algorithms were run for fixed $l = 5$ and $s = 1$. Algorithm 1 was not capable to give results for smaller α_L than $1/16$

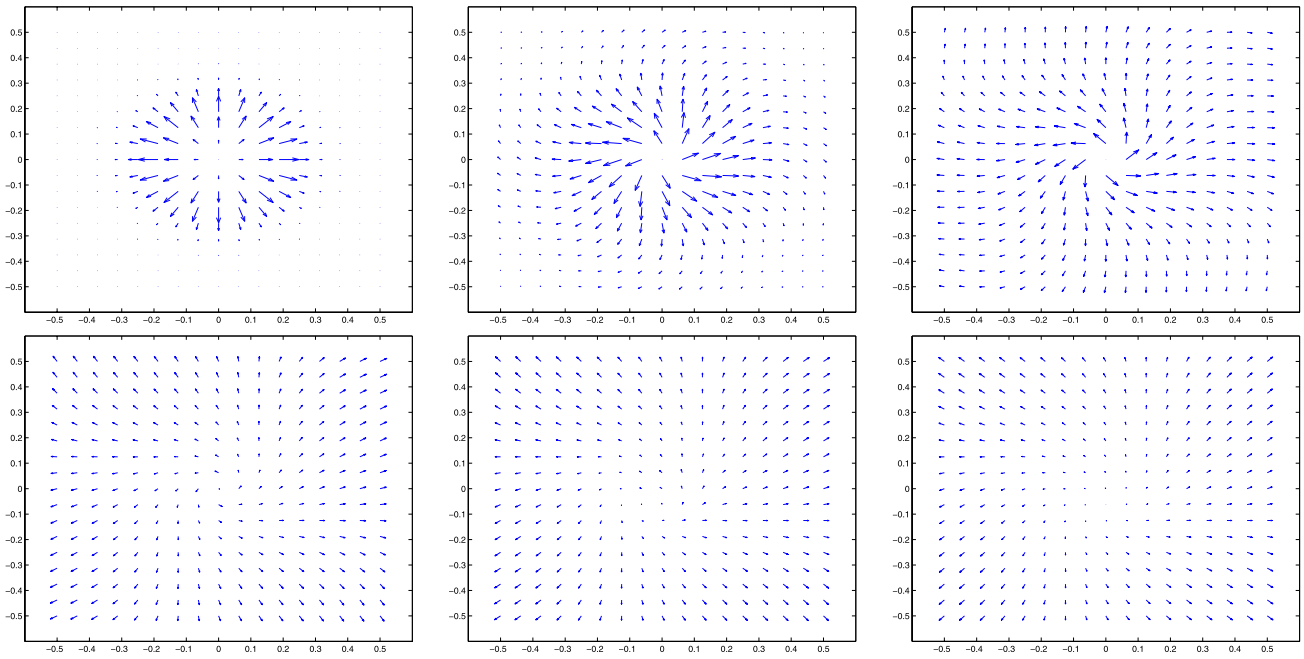

Fig. 9 Numerical approximation of magnetization vector $\mathbf{m}(t,\cdot)$ in Example 3 with $\beta_L = -1, s = 1, l = 4$ and $\alpha_L = 1$ for $t = 0, 0.0119, 0.0295,\ 0.0529, 0.0588, 0.0646$. Copyright © 2006 Society for Industrial and Applied Mathematics. Reprinted from [11] with permission from SIAM Journals

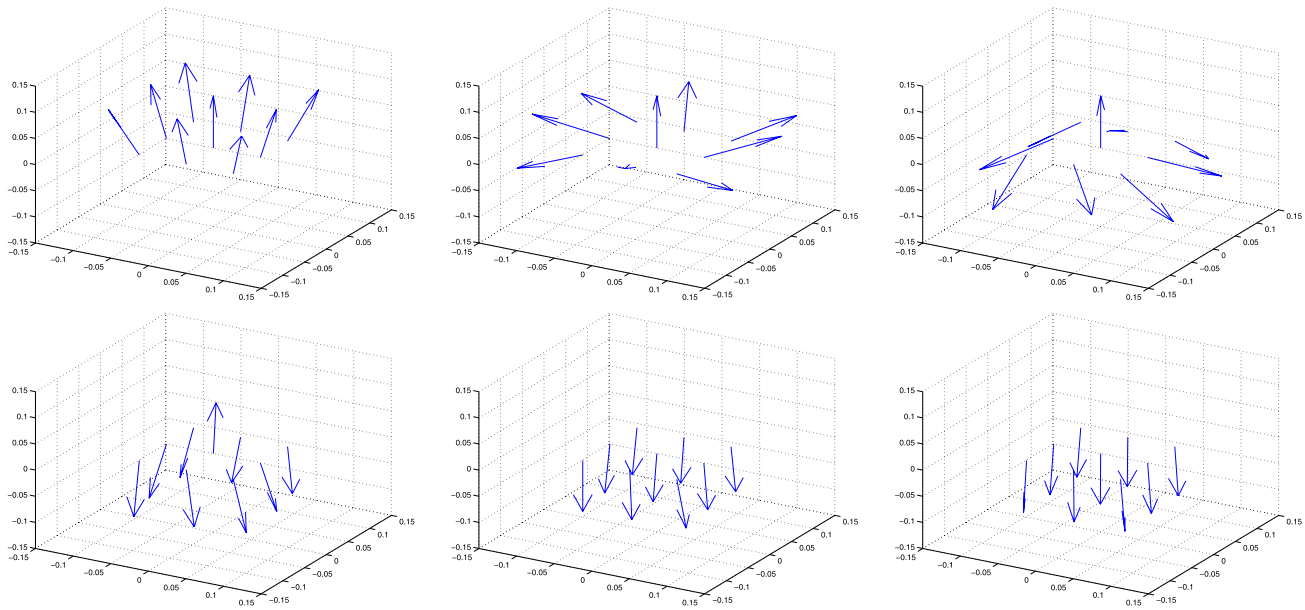

Fig. 10 Nodal values $\mathbf{m}(t,z)$ for nodes z close to the origin in Example 3 with $\beta_L = -1, s = 1, l = 4$ and $\alpha_L = 1$ for $t = 0, 0.0119, 0.0295, 0.0529, 0.0588, 0.0646$. Copyright © 2006 Society for Industrial and Applied Mathematics. Reprinted from [11] with permission from SIAM Journals

while Algorithm 3 ran even for values $\alpha_L = 1,\ 1/4,\ 1/16,\ 1/64,\ 1/256$. The plot in Fig. 12 shows that the blow-up time approaches the time $t \approx 0.06$ for decreasing α_L. The experimental values $\alpha_L = 1/64$ and $\alpha_L = 1/256$ almost coincide.

Better performance of Algorithm 3 compared to Algorithm 1. The results obtained for explicit Algorithm 1 in [42] are similar to the results obtained for implicit Algorithm 3 in [11]. The implicit nature allows for the use of smaller values for α_L which lead to too restrictive conditions on

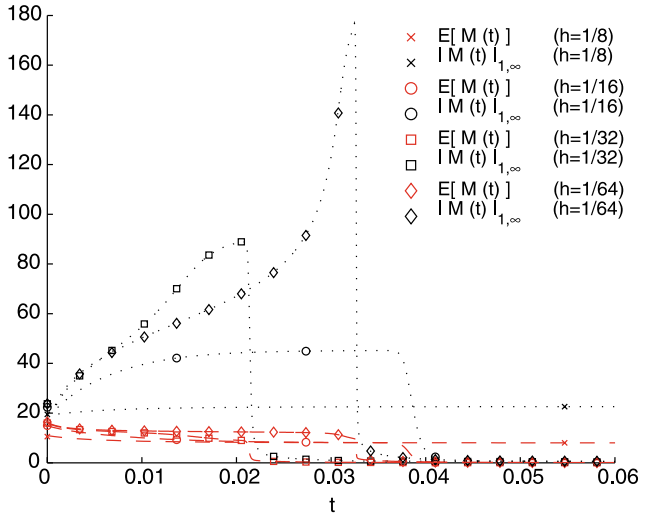

Fig. 11 Energy and $W^{1,\infty}$ semi-norm for decreasing mesh-sizes $h = 1/8, 1/16, 1/32, 1/64$ in Example 3 with $\beta_L = -1, s = 1, l = 5$ and $\alpha_L = 1$. Copyright © 2006 Society for Industrial and Applied Mathematics. Reprinted from [11] with permission from SIAM Journals

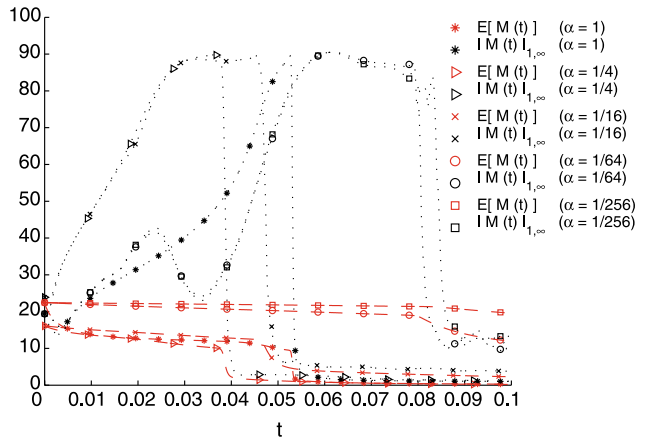

Fig. 12 Energy and $W^{1,\infty}$ semi-norm in Example 3 with $\beta_L = -1$, $s = 1$, $l = 5$ and $\alpha_L = 1, 1/4, 1/16, 1/64, 1/256$. Copyright © 2006 Society for Industrial and Applied Mathematics. Reprinted from [11] with permission from SIAM Journals

the time step size for the explicit Algorithm 1. The total runtimes of the explicit scheme (using reduced integration) and the implicit scheme are comparable. However, for small values of α_L or for three-dimensional problems, the explicit Algorithm 1 from [42] is of limited practical use.

4.3 Standard Problem #1 of μMAG

Next example is derived from a benchmarking problem [53, Problem 1] of a thin uniaxial ferromagnetic film. The numerical simulations taken from [10] are the first simulations

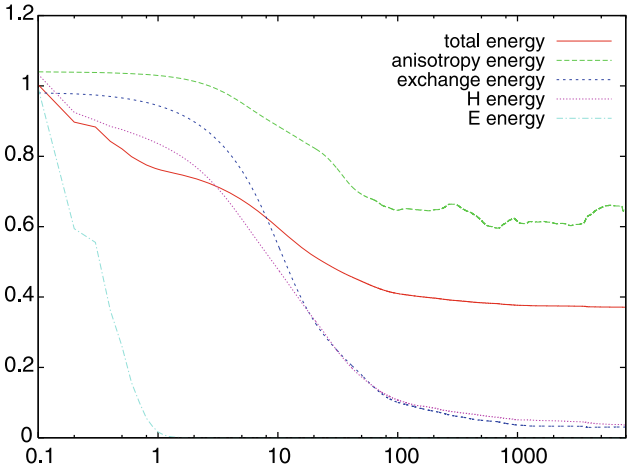

Fig. 13 Evolution of normalized total, anisotropy, exchange, magnetic field and electric field energy in logarithmic scale for the coupled M-LL model, Example 4. Reprinted from [10] with permission from the authors

published in the existing literature modelling the three dimensional case.

The physical model coupling Maxwell equations and the Landau-Lifshitz equation (10)–(12) considers the effective field taking the form

$$\mathbf{H}_{\text{eff}} = A\Delta\mathbf{m} + K\langle \mathbf{m}, \mathbf{p}\rangle + \mathbf{H},$$

with constants

$$A = \frac{2A_{\text{exc}}}{\mu_0 M_s^2}, \qquad K = \frac{2K_{\text{ani}}}{\mu_0 M_s^2}.$$

Example 4 Let $\Omega = (0, 2) \times (0, 1) \times (0, 0.02)$, and $\Omega^{\text{out}} = (-0.2, 2.2) \times (-0.2, 1.2) \times (-0.04, 0.06)$. The domain dimensions are in μm. Further take

$$\alpha = 0.5, \quad \gamma = 2.2 \times 10^9, \quad M_s = 8 \times 10^5, \quad \sigma = 0,$$

$$K_{\text{ani}} = 5 \times 10^2, \quad A_{\text{exc}} = 1.3 \times 10^{-11}, \quad \mathbf{p} = (1, 0, 0),$$

$$\varepsilon_0 = 0.88422 \times 10^{-11}, \quad \mu_0 = 1.25667 \times 10^{-6}.$$

The initial condition $\mathbf{m}^0$ is defined by assigning unit vectors with random orientation to every vortex of the mesh.

More details on space discretization can be found in the above mentioned manuscript. The authors made an interesting comparison of the full Maxwell-LL model with the single LL model. In Fig. 13 you can see the evolution of particular energies for coupled system, whereas in Fig. 14, the corresponding energies for single LL model are depicted. Snapshots of the magnetization at several time instances are depicted in Fig. 15 for coupled M-LL model and in Fig. 16 for single LL model. Clearly, the inclusion

of Maxwell equations does influence the result. In the single LL model, the magnetization is aligned over whole domain while for coupled M-LL model, a formation of domain walls occurred.

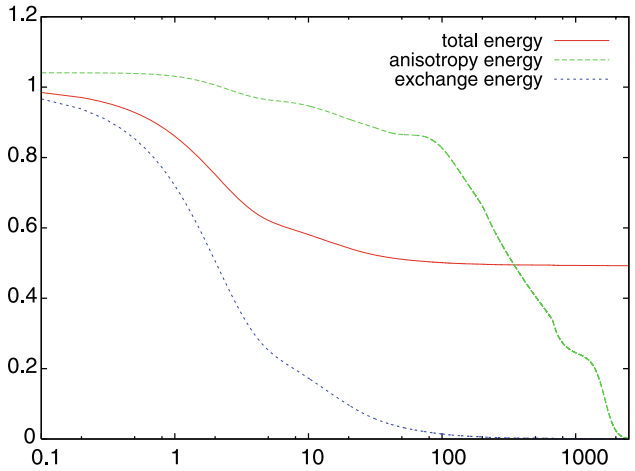

Fig. 14 Evolution of normalized total, anisotropy and exchange energy in logarithmic scale for the single LL model, Example 4. Reprinted from [10] with permission from the authors

4.4 Adaptivity

Only recently there was done some work in the rigorous analysis of adaptive methods for micromagnetics. Baňas provides a posteriori estimates for the error indicators that can be used for numerical schemes dealing with the LL equation.

In [54] Baňas studies the LL equation for the case of effective field consisting of exchange field and applied field, thus $\mathbf{H}_{\text{eff}} = \Delta\mathbf{m} + \mathbf{H}_{\text{app}}$.

Discretization of the time interval with n different time steps τ_i gives an approximate solutions denoted by $\mathbf{m}^i, \mathbf{H}^i$. For space discretization a regular triangulation $\mathcal{T}_i$ of the domain on every time step were used. Then a space of element-wise linear functions was used for approximation of $\mathbf{m}$.

The results from the computational tests from Sect. 4 suggest, that semi-implicit scheme (31) with projection back onto sphere is a good candidate for a reliable scheme dealing with mesh adaptivity. We go further and since this scheme is a semi-implicit scheme, we hope that fully-implicit scheme will perform even better. Of course, we need to re-normalize the computed approximate solution after each time step and project it back onto sphere.

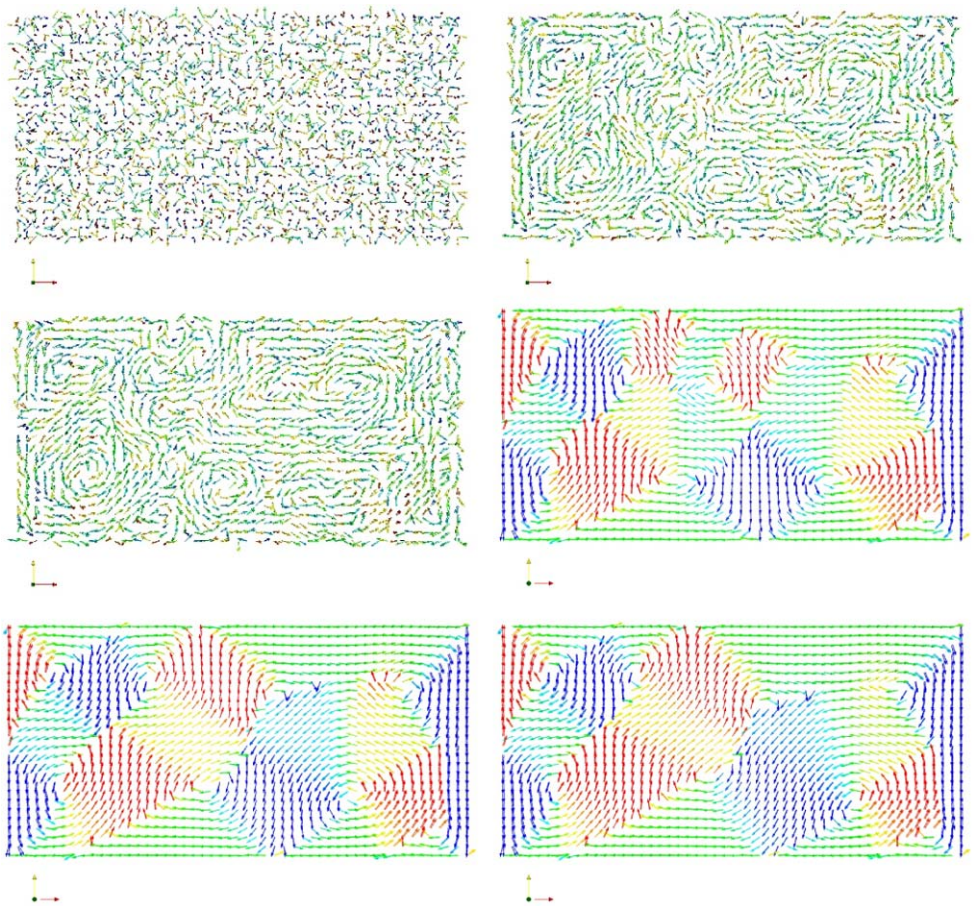

Fig. 15 Snapshots of the magnetization pattern of the coupled M-LL model at the time instances $t = 0$, 100, 200, 2500, 5000, 8000. Reprinted from [10] with permission from the authors

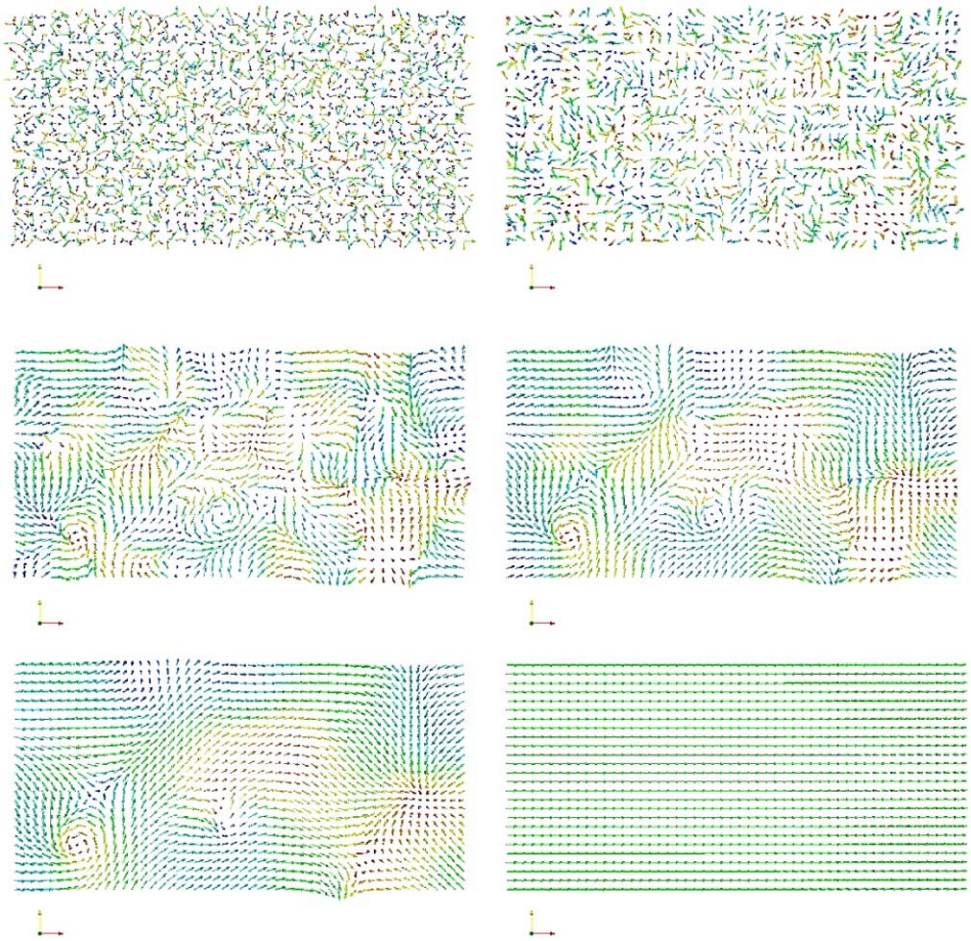

Fig. 16 Snapshots of the magnetization pattern of the single LL model at the time instances $t = 0$, 10, 50, 100, 200, 2500. Reprinted from [10] with permission from the authors

For the comparison, we take recent Bartels-Prohl Algorithm 3.

The following error indicators serve as good thresholds for refinement or coarsening

$$\mu_i^\tau = \|\mathbf{m}^i - \mathbf{m}^{i-1}\|_{H^1}^2 + \int_{t_i-1}^{t_i} \|\mathbf{H}_{\text{app}} - \mathbf{H}^i\|^2,$$

$$\begin{aligned}\mu_{K,i}^h = &\sum_{e\subset K} h_e \|[\nabla \mathbf{m}^i \cdot \nu_e]_e\|_{L^2(e)}^2 \\ &+ \|h_K |\nabla \mathbf{m}^i|^2 \mathbf{m}^i\|_{L^2(K)}^2 + \left\| h_K \frac{\mathbf{m}^i - \mathbf{m}^{i-1}}{\tau_i} \right\|_{L^2(K)}^2 \\ &+ \|h_K (\mathbf{H}^i - \mathbf{H}^{i-1})\|_{L^2(K)}^2,\end{aligned}$$

where h_K stands for the diameter of the element K and h_e denotes the length of edge e. Further, ν_e is the unit outward normal vector to the triangle K on $e \in \partial K$ and $[\cdot]_e$ denotes the jump along the edge e. The a posteriori error estimates for the error indicators were derived in [55] and read as

$$\|\mathbf{m}(t_i) - \mathbf{m}^n(t_i)\|^2 \le \|\mathbf{m}(0) - \mathbf{m}^0\|^2 + \|\mathbf{H}(0) - \mathbf{H}^0\|^2 + C \sum_{j=1}^{i} \tau_j (\mu_j^\tau + \mu_j^h),$$

where $\mathbf{m}^n(t)$ is time-dependent linear interpolation of the discretized solution $\mathbf{m}^i$ for $i = 0, \ldots, n$ and $\mathbf{m}^0, \mathbf{H}^0$ denote suitable approximations of initial data.

Using the previous error indicators Baňas proposed the following adaptive algorithm

Algorithm 11

1. *Set* $\tau_i = \tau_{i-1}, \mathcal{T}_i = \mathcal{T}_{i-1}$.
2. *Set* $t_i = t_{i-1} + \tau_i$ *and compute the discrete solution by one of the compared schemes. If* $\mu_i^\tau \le \varepsilon_\tau^r TOL$ *proceed with the space refinement step* 3, *otherwise decrease* τ_i *and repeat step* 1.
3. *For all* $K \in \mathcal{T}_i$, *if* $\mu_{K,i}^h > \varepsilon_h^r TOL/N_i$ *mark* K *for refinement, if* $\mu_{K,i}^h < \varepsilon_h^c TOL/N_i$ *mark* K *for coarsening.*
4. *Refine/coarsen mesh and compute new solution, if* $\mu_i^\tau \le \varepsilon_\tau^c TOL$ *increase* τ_i *and go to step* 2 *otherwise proceed with next time level and go to step* 1 *of the algorithm.*

The constants $\varepsilon_\tau^r, \varepsilon_h^r, \varepsilon_\tau^c$ are chosen according to performance of the algorithm, N_i is number of elements from $\mathcal{T}_i$.

Numerical Example

The problem of finite blow-up appeared in [11, 42] for uniform meshes was recomputed in [54] using adaptive strategy described above. This particular example features a finite time blow-up of the solution and can therefore serve as a good case study for adaptive algorithms.

Example 5 The domain is considered to be a square $\Omega = (-1/2, 1/2) \times (-1/2, 1/2)$ with vanishing applied field $\mathbf{H}_{\text{app}}$ and following initial condition

$$\mathbf{m}_0(\mathbf{x}) = \begin{cases} (0, 0, -1) & \text{for } |\mathbf{x}| \geq 1/2, \\ (2\mathbf{x}A,\, A^2 - |\mathbf{x}|^2)/(A^2 + |\mathbf{x}|^2) & \text{for } |\mathbf{x}| \leq 1/2, \end{cases}$$

where $A = (1-2|\mathbf{x}|)^4/16$. The magnetization vector evolves in such a way that in finite time a singularity with respect to $\|\nabla \mathbf{m}\|_\infty$ occurs in the middle of the square and the direction of $\mathbf{m}$ flips from upwards to downwards which results in the jump of the energy measured by $\nabla \mathbf{m}$.

Results from [54] indicate that for both compared schemes, the adaptive algorithm localized the position of the singularity and increased the efficiency of the performed computations. Moreover, both methods were robust enough to increase the time-stepping $\tau = \mathcal{O}(h^2)$ used in [11].

5 Conclusions and Outlook

Although a significant progress has been done in the last three years in the field of numerical approximation of weak solutions, there still remain open questions that need an answer. To list some of them:

Design of a *linear* scheme conserving the length of $\mathbf{m}^i$, converging to the weak solution of the LL equation (for the case when the exchange field is included). Nowadays, the schemes mentioned in Sects. 3.3–3.7 are all nonlinear and for all of them, inner iterations mostly based on a contraction argument are needed in computational implementations.

Convergence of *whole* sequence to the weak solution. For all schemes dealing with weak solutions, a subconvergence to the solution has been proved. The question is if it is possible to prove convergence of the whole sequence or even to derive error estimates. Alternatively, one can seek for a new scheme for which this is possible.

Study of *inverse problems* in the micromagnetics. Rising significance of magnetic recording demand better performance of micromagnetic systems. This can be achieved by optimization of different parameters or geometry. As already pointed out in Sect. 1.4.4, a key role in optimization and inverse problems is sensitivity analysis of the LL equation. Therefore, its study can bring fruitful improvements in the design of nanodevices.

References

1. Kružík M, Prohl A (2006) Recent developments in the modeling, analysis, and numerics of ferromagnetism. SIAM Rev 48:439–483
2. Bertotti G (1998) Hysteresis in magnetism. Academic Press, San Diego
3. Landau L, Lifshitz E (1935) On the theory of the dispersion of magnetic permeability in ferromagnetic bodies. Phys Z Sowjetunion 8:153–169
4. Gilbert T (1955) A Lagrangian formulation of gyromagnetic equation of the magnetization field. Phys Rev 100:1243–1255
5. d'Aquino M, Serpico C, Miano G (2005) Geometrical integration of Landau-Lifshitz-Gilbert equation based on the mid-point rule. J Comput Phys 209:730–753
6. Prohl A (2001) Computational Micromagnetism. Advances in numerical mathematics. Teubner, Stuttgart
7. Cimrák I (2005) Error estimates for a semi-implicit numerical scheme solving the Landau-Lifshitz equation with an exchange field. IMA J Numer Anal 25:611–634
8. Podio-Guidugli P (2001) On dissipation mechanisms in micromagnetics. Eur Phys J B 19:417–424
9. Monk P, Vacus O (2001) Accurate discretization of a nonlinear micromagnetic problem. Comput Methods Appl Mech Eng 190:5243–5269
10. Baňas L, Bartels S, Prohl A. (2008) A convergent implicit discretization of the Maxwell-Landau-Lifshitz-Gilbert equation. SIAM J Numer Anal (accepted). http://na.uni-tuebingen.de/pub/prohl/papers/mllg.pdf
11. Bartels S, Prohl A (2006) Convergence of an implicit finite element method for the Landau-Lifshitz-Gilbert equation. SIAM J Numer Anal 44:1405–1419
12. Brown W (1963) Thermal fluctuations of a single domain particle. Phys Rev 130:1677–1686
13. Kubo R, Toda M, Hashitsume N (1991) Nonequilibrium statistical mechanics. Statistical physics, vol 2. Springer, Berlin
14. Tsiantos V, Scholz W, Suess D, Schrefl T, Fidler J (2002) The effect of the cell size in Langevin micromagnetic simulations. J Magn Magn Mater 242–245:999–1001
15. Garcia-Palacios L, Lazaro FJ (1998) Langevin-dynamics study of the dynamical properties of small magnetic particles. Phys Rev B 58:14937–14958
16. Scholz W, Schrefl T, Fidler J (2001) Micromagnetic simulation of thermally activated switching in fine particles. J Magn Magn Mater 233:296–304
17. Cheng XZ, Jalil MBA, Lee HK, Okabe Y (2006) Mapping the Monte-Carlo scheme to Langevin dynamics: A Fokker-Planck approach. Phys Rev Lett 96:067208
18. Baňas L, Prohl A, Slodička M. Modeling od thermally assisted magnetodynamics. Preprint, http://na.uni-tuebingen.de/pub/prohl/papers/thermagA5.pdf
19. Cimrák I, Melicher V (2007) Sensitivity analysis framework for micromagnetism with application to optimal shape design of MRAM memories. Inverse Probl 23:563–588
20. Cimrák I, Melicher V (2006) The Landau-Lifshitz model for shape optimization of MRAM memories. PAMM 6:23–26

21. Tai X, Chan T (2004) A survey on multipole level set methods with applications for identifying piecewise constant functions. Int J Numer Anal Model 1:25–47
22. Melicher V, Cimrák I, Van Keer R (2008) Level Set Method for optimal shape design of MRAM core. Micromagnetic approach. Physica B: Condens Matter 403:308–311
23. Carbou G, Fabrie P (2001) Regular solutions for Landau-Lifshitz Equation in a bounded domain. Diff Integral Equ 14:213–229
24. Guo B, Ding S (2001) Neumann problem for the Landau-Lifshitz-Maxwell system in two dimensions. Chin Ann Math Ser B 22:529–540
25. Lewis D, Nigam N (2003) Geometric integration on spheres and some interesting applications. J Comput Appl Math 151:141–170
26. E W, Wang X-P (2000) Numerical methods for the Landau-Lifshitz equation. SIAM J Numer Anal 38:1647–1665
27. Krishnaprasad P, Tan X (2001) Cayley transforms in micromagnetics. Physica B 306:195–199
28. Lewis D, Nigam N (2000) A geometric integration algorithm with applications to micromagnetics. Technical Report 1721, IMA preprint series
29. Monk P, Vacus O (1999) Error estimates for a numerical scheme for ferromagnetic problems. SIAM J Numer Anal 36:696–718
30. Serpico C, Mayergoyz I, Bertotti G (2001) Numerical technique for integration of the Landau-Lifshitz equation. J Appl Phys 89:6991–6993
31. Cimrák I (2007) Error analysis of numerical scheme for 3D Maxwell-Landau-Lifshitz system. Math Methods Appl Sci 30:1667–1683
32. Cimrák I (2007) Existence, regularity and local uniqueness of the solutions to the Maxwell-Landau-Lifshitz system in three dimensions. J Math Anal Appl 329:1080–1093
33. Cimrák I (2008) Regularity properties of the solutions to the 3D Maxwell-Landau-Lifshitz system in weighted Sobolev spaces. J Comput Appl Math 215:320–327
34. Alouges F, Soyeur A (1992) On global weak solutions for Landau-Lifshitz equations: Existence and nonuniqueness. Nonlinear Anal 18:1071–1094
35. Guo B, Hong M (1993) The Landau-Lifshitz equation of the ferromagnetic spin chain and harmonic maps. Calc Var Partial Differ Equ 1:311–334
36. Slodička M, Cimrák I (2003) Numerical study of nonlinear ferromagnetic materials. Appl Numer Math 46:95–111
37. Cimrák I, Slodička M (2004) An iterative approximation scheme for the Landau-Lifshitz-Gilbert equation. J Comput Appl Math 169:17–32
38. Cimrák I, Slodička M (2004) Optimal convergence rate for Maxwell-Landau-Lifshitz system. Physica B 343:236–240
39. Slodička M, Baňas L (2004) A numerical scheme for a Maxwell-Landau-Lifshitz-Gilbert System. Appl Math Comput 158:79–99
40. Slodička M, Cimrák I (2004) Improved error estimates for a Maxwell-Landau-Lifshitz system. PAMM 4:71–74
41. Alouges F, Jaisson P (2006) Convergence of a finite element discretization for the Landau-Lifshitz equations in micromagnetism. Math Models Methods Appl Sci 16:299–316
42. Bartels S, Ko J, Prohl A (2007) Numerical approximation of the Landau-Lifshitz-Gilbert equation and finite time blow-up of weak solutions. Math Comput (accepted)
43. Barret J, Bartels X, Feng S, Prohl A (2007) A convergent and constraint-preserving finite element method for the p-harmonic flow into spheres. SIAM J Numer Anal 45:905–927
44. Bartels S (2006) Constraint preserving, inexact solution of implicit discretizations of Landau-Lifshitz-Gilbert equations and consequences for convergence. PAMM 6:19–22
45. Bartels S, Prohl A (2007) Constraint preserving implicit finite element discretization of harmonic map heat flow into spheres. Math Comp 76:1847–1859
46. Bartels S (2004) Stability and convergence of finite element approximation schemes for harmonic maps. SIAM J Numer Anal 43:220–238
47. Bartels S, Prohl A, Lubich C. Convergent discretization of heat and wave map flows to spheres using approximate discrete Lagrange multipliers. Preprint
48. Bartels S, Prohl A. Convergence of an implicit, constraint preserving finite element discretization of p-harmonic heat flow into spheres. Preprint
49. Monk P (2003) Finite element methods for Maxwell's equations. Numerical mathematics and scientific computation. Oxford University Press, London
50. Carbou G, Fabrie P (2001) Time average in micromagnetism. J Differ Equ 147:383–409
51. Baňas L (2005) Numerical methods for the Landau-Lifshitz-Gilbert equation. In: Li Z, Vulkov L, Wasniewski J (eds) Numerical analysis and its applications: third international conference, NAA 2004, Rousse, Bulgaria, vol 3401. Springer, Berlin, p 158
52. Mayergoyz I, Serpico C, Shimizu Y (2000) Coupling between eddy currents and Landau-Lifshitz dynamics. J Appl Phys 87:5529–5531
53. Webpage address: http://www.ctcms.nist.gov/~rdm/mumag.org.html
54. Baňas L (2005) Adaptive methods for dynamical micromagnetics. In: Bermúdez de Castro A, Gómez D, Quintela P, Salgado P (eds) Proceedings of ENUMATH 2005, Santiago de Compostela, Spain. Springer, Berlin
55. Baňas L (2004) On dynamical micromagnetism with magnetostriction. Ghent University, Belgium, PhD thesis, http://cage.ugent.be/~lubo/